3.2.6.II Current Pulses in the Electronegative Glow Phase of the SF_6 Spark and in the corresponding D.C. Glow Discharge

3.2.6.II(i) General description of the pulses under both spark and d.c. conditions

Within certain ranges of applied voltage and gas pressure, sharp current pulses are observed to occur in the electronegative glow phase of the SF_6 spark. These pulses appear on the oscillograms of Fig. 3.2.2.(iv)a and b, which depict current and voltage development in a 0.8 Torr SF_6 spark, pulsed in the metre-gap at 12.00 kV and 12.50 kV. In Fig. 3.2.2.(iv)a, the current pulses are seen to decrease in amplitude with time from about 100 mA, and to increase in frequency from about 40 kHz, until they eventually disappear at a time just before the transition to the dissociated glow phase. This trend is accompanied by a very gradual increase in the base-current on which the pulses are superimposed. This base-current is not well resolved in Fig. 3.2.2.(iv)a, but averages about 5 mA and attains a value of approximately 20 mA when the pulses disappear. Another feature that is difficult to resolve in this figure is an increase in the width of the current pulses with increasing base-current and frequency. From Fig. 3.2.2.(iv)b, it can be seen that compared to the 12.00 kV spark, the base-current in the 12.50 kV spark is larger, the average pulse frequency is higher, and the pulse amplitudes are generally lower. This oscillogram highlights the fact that the pulses are obtained only within a limited range of discharge base-current. By increasing the applied gap voltage, the base-current amplitude increases to a stage where no current pulses are observed. This can be seen in Fig. 3.2.2.(iv)c. For a particular set of experimental conditions, the pulses have been found to be very repeatable from shot-to-shot provided a fresh fill of SF_6 is admitted after every three or four shots.

Because the results of some initial experiments designed to obtain information on the spark current pulses proved inconclusive, it was decided to look for the pulses under d.c. conditions. A greater range of experimental techniques is available under d.c. conditions and in general d.c. results are

less difficult to interpret. It turns out that current pulses do occur in low pressure d.c. SF_6 discharges at similar currents and voltages to those encountered in the electronegative glow phase of the SF_6 spark.

The d.c. discharge circuit used consisted of a stabilized power supply (Hipotronix, Model 810-100) connected in series with the metre-gap via a 517 kΩ resistor. The cathode was connected directly to ground, and the discharge current measured by means of a commercial current probe (Tektronix, Model P6042) attached around the lead connecting cathode and ground. The gap voltage was measured using a 1000 X voltage attenuator (Tektronix, Model P6015) connected between the discharge anode and ground. With the SF_6 pressure at 0.80 Torr, a d.c. discharge was maintained in the metre-gap with a supply voltage of + 11 kV. Current pulses and corresponding voltage oscillations of regular amplitude and frequency were observed to occur. Figures 3.2.6.(i)a and b show these variations on different time and amplitude scales. They show that when the gap voltage reaches 9.6 kV, a current pulse of amplitude 200 mA and width 1.5 μs occurs, accompanied by a collapse in the gap voltage from 9.6 kV to 7.6 kV. The discharge current then remains constant at approximately 3 mA for about 24 μs during which time the gap voltage gradually increases back to 9.6 kV. When this voltage is attained, the process is repeated. Current and voltage waveforms of similar appearance were obtained in the movable-electrode chamber using the same d.c. circuit. The variations of current pulse amplitude and frequency with base-current were measured in a 2.5 Torr d.c. SF_6 discharge of length 11 cm. The results are plotted in Fig. 3.2.6.(ii). At very low base-currents ($\lesssim$ 2 mA) the discharge appears diffuse and no pulses are observed. Once the discharge current is raised to about 2 mA, a partial constriction is seen to extend about one-third the distance into the gap from the cathode end and current pulses of relatively low amplitude (18 mA) and frequency (12 kHz) are observed. When the base-current is very slightly increased above the pulse threshold value, the constriction extends further into the column and is accompanied by a sharp

Fig. 3.2.6.(i)a Oscillogram showing the current trace (upper) and voltage trace (lower) for a 0.80 Torr d.c. SF_6 discharge maintained in the metre-gap, for a supply voltage of 11.0 kV and a series resistance of 517 kΩ.

Fig. 3.2.6.(i)b Oscillogram showing the same traces shown in Fig. 3.2.6.(i)a on a much slower sweep speed.

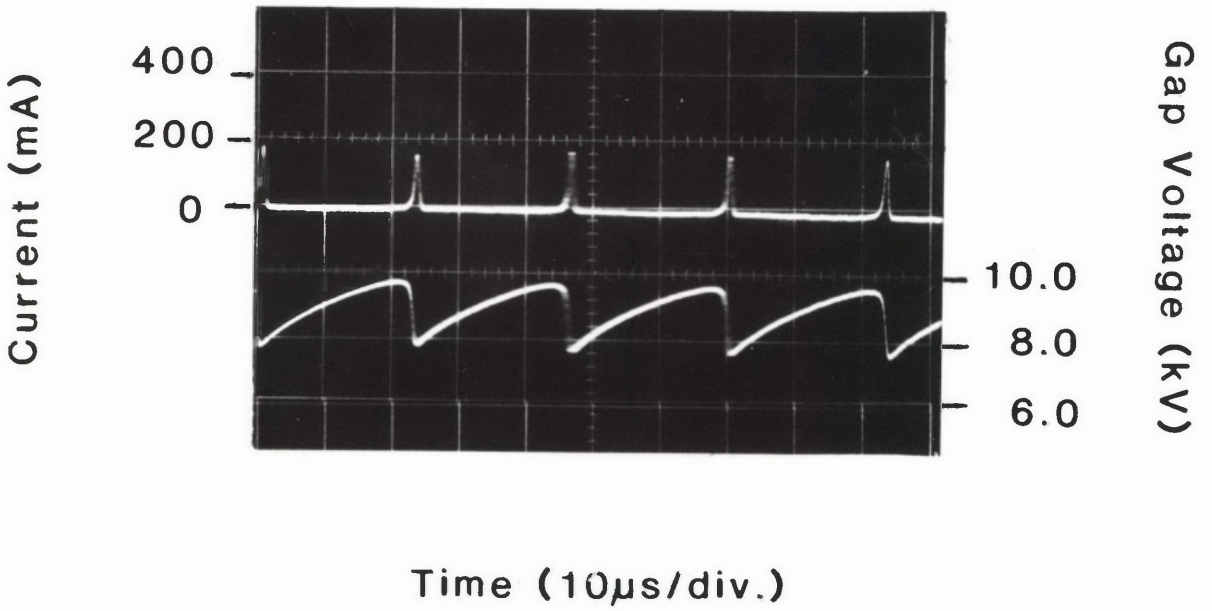
Current (mA)
400
200
0
10.0
8.0
6.0
Gap Voltage (kV)
Time (10μs/div.)

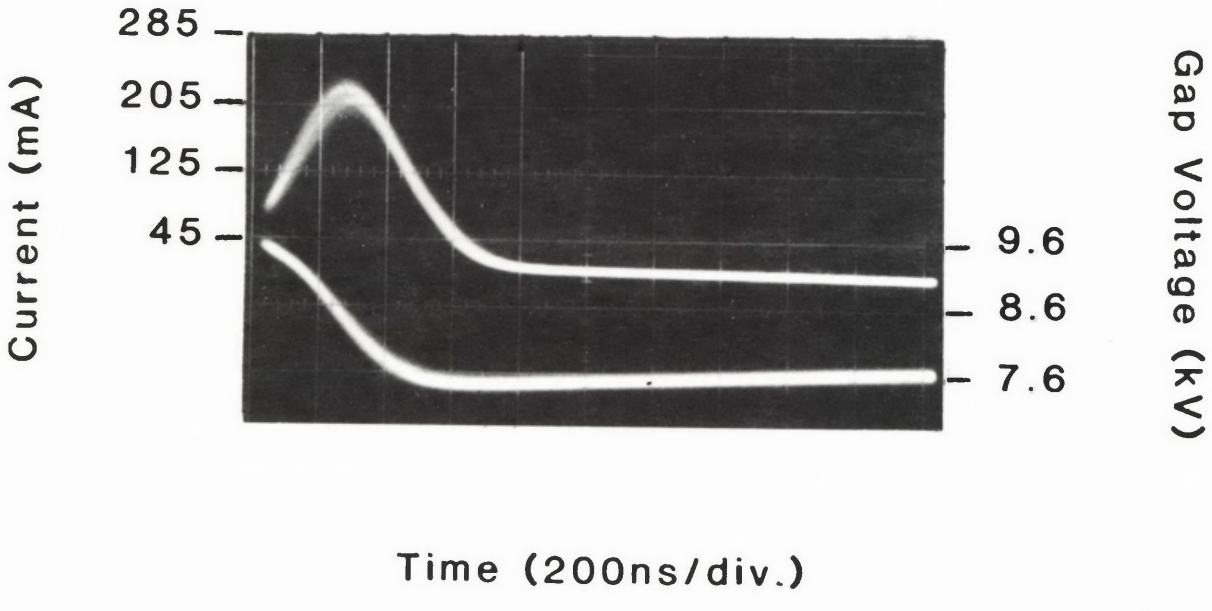
Current (mA)
285
205
125
45
9.6
8.6
7.6
Gap Voltage (kV)
Time (200ns/div.)

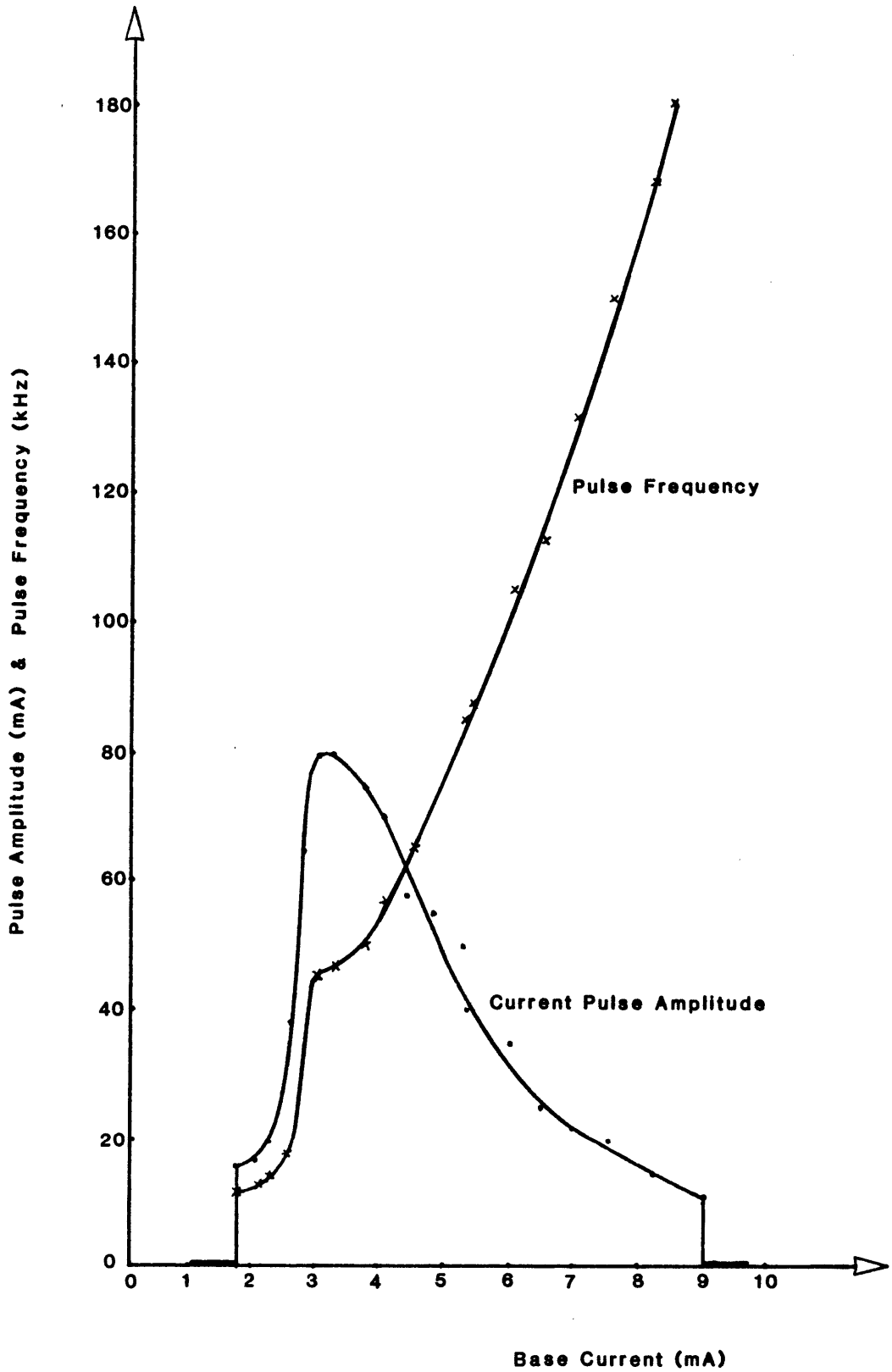

Fig. 3.2.6.(ii) Current pulse amplitude and frequency as a function of base-current in a 2.5 Torr, 11 cm d.c. SF_6 discharge.

increase in current pulse amplitude and frequency. At a discharge current of about 3 mA the pulse amplitude attains a maximum value of about 80 mA. At this stage the constriction (of diameter $\sim$ 5 mm) extends to within a few mm of the anode, the surface of which remains covered by a thin, diffuse layer of luminosity. The pulse amplitude then decreases as the base-current is further raised, while the pulse frequency continues to increase until it attains a value of approximately 200 kHz at a base-current of 9 mA. Beyond this base-current, no pulses are observed. The pulse width is observed to increase from about 500 ns at threshold, to about 4 μs just before pulse extinction. It appears that pulse extinction occurs when the pulse width and interpulse period become approximately equal.

The general variations described above in the current pulse width, frequency and amplitude with base-current in the d.c. SF_6 discharge, together with the existence of an upper base-current limit beyond which the current pulses are not observed, are consistent with the pulse properties observed in the spark discharge. The pulses observed in the low pressure SF_6 discharge under spark and d.c. conditions appear therefore to be the result of the same discharge processes.

In the following sub-sections, II(ii), (iii) and (iv), a description is given of a series of experiments, in which macroscopic measurements are made on the current pulses, under both spark and d.c. conditions. In II(v), a description is given of a series of experiments which provides information regarding fundamental properties of the positive column, where, it turns out, the current pulses have their origin. In II(vi), the experimental results are discussed and conclusions are made regarding the processes which generate the current pulses.

3.2.6.II(ii) An investigation of the role of the external circuit

(a) *Spark circuit*

Despite the evidence suggesting that the pulses occurring in both the spark and d.c. discharges are due to the same fundamental processes, a check was made to confirm that the pulses in the spark are not due to any instability

associated with the thyratron unit. The CX1140 hydrogen thyratron was physically disconnected from the metre-gap circuit and was replaced with the mechanical safety switch, S, shown in Fig. 2.2.1. It was found that the current pulses still occurred when this switch was used to pulse the gap.

An investigation was then made to determine whether the current pulses could be obtained in the movable-electrode chamber using the 3C45 thyratron pulsing circuit (see Fig. 2.2.1.). It was found that because the current pulses are obtained only within a limited range of current and voltage in the electronegative glow phase, it was not possible to produce them using this low voltage ($\lesssim$ 3 kV) pulsing circuit. In order to produce an electronegative glow phase which has current pulses, it was necessary to use the higher voltage (CX1140 thyratron) circuit with appropriate series resistances. Figure 3.2.6.(iii) shows, for example, the current and voltage pulses obtained in a 1.96 Torr SF_6 spark fired in a 20 cm gap at 5.43 kV, using the metre-gap circuitry as shown in Fig. 2.2.1. The average base-current is seen in this case to be approximately 4.5 mA, while the average current and voltage pulse amplitudes are approximately 8 mA and 50 volts, respectively (here the gap voltage has been measured with the aid of the Tektronix, type Z plug-in unit mentioned in Section 2.3.1.).

(b) *D.C. circuit*

To examine any roles played by series resistance, inductance and capacitance in the behaviour of the current pulses, these circuit components were individually varied. The series resistance was varied between 517 kΩ and 1.5 MΩ while maintaining the base-current in a 2.5 Torr, 11 cm discharge, constant at 3 mA. As expected, the base-current and current pulse-height decreased with increasing resistance. However, changing resistance had little effect on the pulse frequency.

Using a fixed series resistance of 517 kΩ, a fixed gap of 11 cm and a base-current of 3mA, inductance was added in series with the discharge tube, in the range 2 mH to 50 mH. No variation in the pulse frequency or amplitude was observed over the entire range of added inductance. Damped, high frequency oscillations were found to occur however in the interpulse phase, with their frequency being proportional to $\frac{1}{\sqrt{L}}$. These findings suggest that the current pulses are not due to the electrical instability which can sometimes occur in

Fig. 3.2.6.(iii) Oscillogram showing the current pulses (upper) and voltage pulses (lower) found in the electronegative glow phase of a 1.96 Torr SF_6 spark pulsed in a 20 cm gap at 5.43 kV.

Gap Voltage (kV)
-5.28
-5.33
-5.38
-5.43
0
11
22
33
44
Current (mA)
Time (200μs/div.)

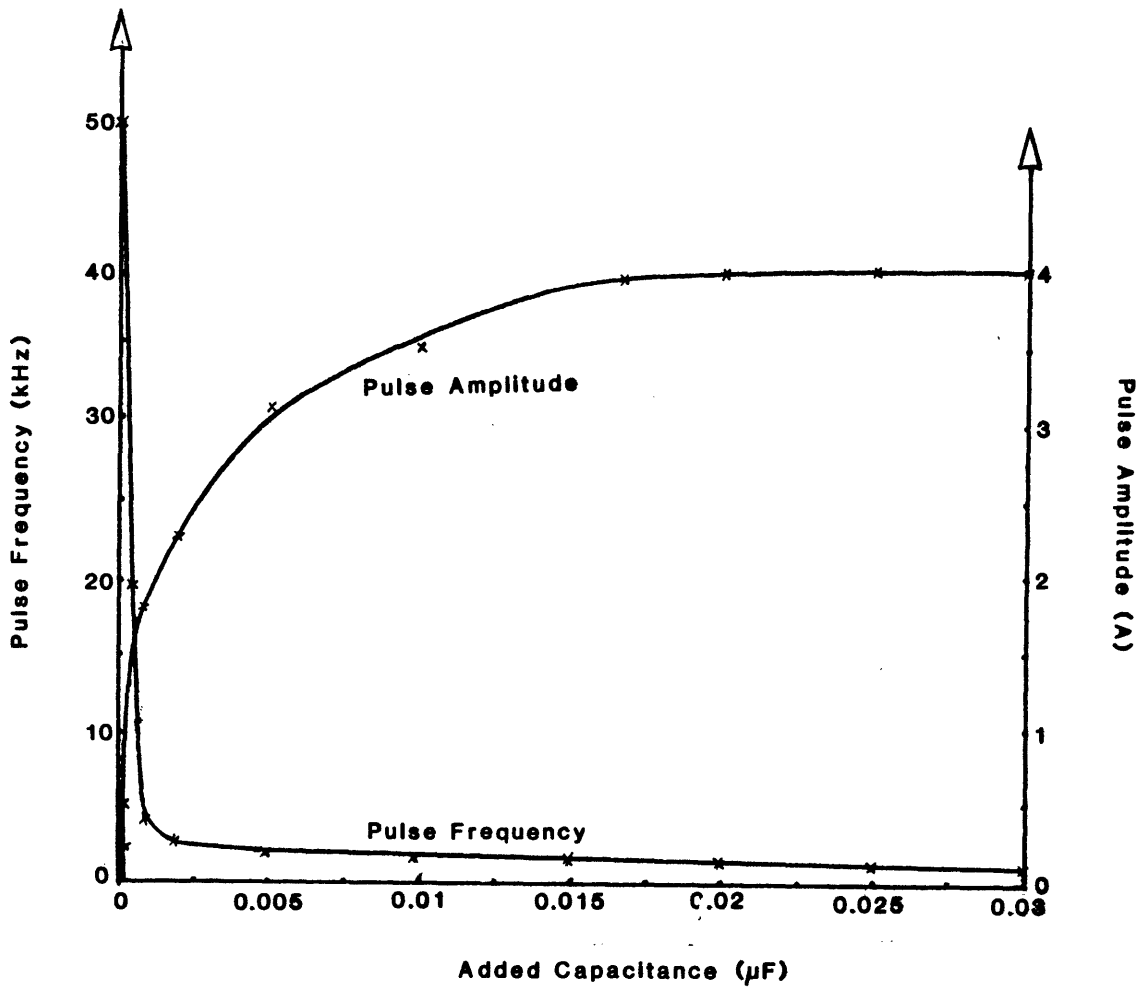

Fig. 3.2.6.(iv) Current pulse amplitude and frequency as a function of added capacitance across an 11 cm gap, in which a 2.5 Torr d.c. SF_6 discharge is maintained at a base-current of 3 mA.

circuits associated with discharges having a negative dynamic resistance (Seeliger, 1944; Reich, 1939). It has not been necessary to examine the dynamic i-V characteristics for the discharges presently studied, since it is known that the frequency of oscillations induced in circuits due to elements with negative dynamic resistance, is significantly affected by variations in the net circuit inductance (Reich, 1939).

Finally, the effect of the addition of capacitance in parallel with the 2.5 Torr, 11 cm gap was observed, again keeping the discharge current constant at 3 mA. The effect on the current pulse amplitude and frequency is shown in Fig. 3.2.6.(iv). As the magnitude of the added capacitance is increased (over the range, 50 pF to 30000 pF), the pulse amplitude increases into the ampere range, and the frequency sharply decreases. Beyond a certain capacitance ($\sim$ 15000 pF) however, the pulse amplitude saturates at a value of 4A. For constant pressure, gap-length and base-current, it is observed that the gap voltage reaches the same value at the onset of a current pulse, irrespective of the magnitude of added capacitance. Two significant points emerge from this capacitance data. One is that the current pulses appear to be triggered at a critical discharge voltage, although the time taken to re-establish this voltage after a current pulse, is controlled by C. The second point is that with increasing capacitance, the current pulse amplitude eventually reaches a saturation value which is of the order of 10^3 times the base-current. These results will be used later in conjunction with the results of II(v) to provide an explanation for the fundamental mechanism producing the current pulses.

3.2.6.II(iii) A search for travelling waves

(a) *Axial propagation*

The possibility of the current pulses being related to the rapid propagation of ionization waves down the discharge tube has been examined. The existence of ionization waves of kiloHertz frequency in the positive column of low pressure glow discharges is well known (Garscadden, 1978). Ishikawa and Suganomata (1976), Suganomata and Ishikawa (1978) and Ishikawa *et al.*

(1979), studying d.c. glow discharges in low pressure SF_6, have reported current oscillations somewhat similar in amplitude, width and period to those obtained in the present work, and have interpreted them as waves propagating through the positive column from the anode- to cathode-end at velocities between 10^7 cm s^{-1} and 10^8 cm s^{-1}. Ishikawa *et al.* observed a phase difference between voltage oscillations induced in two capacitative probes set at different positions along the discharge tube. These probes each consisted of a copper wire wound in a closed circle around the discharge tube and connected to a dual beam oscilloscope via a 0.001 μF capacitor. The authors also observed that the oscillations increased in amplitude in propagating from anode to cathode. They were unable to account for the mechanism of their wave, but suggested that it may be an ion-acoustic shock wave, or one similar to the so-called "soliton" wave.

In an attempt to detect wave propagation in the present work, the electronegative glow phase of the spark as well as the d.c. glow discharge have been examined using a pair of photomultipliers, while the d.c. glow has also been examined using a pair of capacitative probes.

For the SF_6 spark study, the photomultipliers were placed normal to the one-metre discharge tube, 5 cm from either electrode. A 0.8 Torr spark was pulsed at 12.00 kV, providing current pulses similar to those in Fig. 3.2.2.(iv)a. The light pulses which accompany the current pulses were observed on the Tektronix, type 551 dual-beam oscilloscope, and a phase difference was looked for between the response of the two photomultipliers to a particular current pulse. The photomultipliers used were an EMI, type 9658A model with an S-20 photocathode response (320-850 nm) and an EMI, type 9789QB model with an S-11, extended u.v. response (175-630 nm). Each photomultiplier had an anode pulse rise-time of less than 10 ns. Using neutral density filters, the response of both photomultipliers was checked and found to be linear to within 5%. To the front end of each photomultiplier, was attached a cylindrical tube of length 20 cm, which housed a set of three equally-spaced optical stops with centrally located pinhole apertures. These apertures were each 1 mm in

diameter and were arranged to be in line with the photomultiplier tube axis. The inner walls of the aperture housing were blackened with a fine coat of carbon powder, in order to ensure that only that light emitted by the discharge directly in line with the photomultiplier axis, would fall on the photocathode. This was achieved by placing the photomultipliers and their aperture housings directly against the discharge tube (the maximum solid angle subtended by the aperture arrangement was less than 10^{-4} steradians).

Since the pulses in the 0.8 Torr, 12 kV spark commence more than 80 μs after breakdown, it was necessary to delay the external triggering of the oscilloscope with respect to the instant of gap voltage application, in order to obtain nanosecond resolution of the light pulses. This was done using a suitable delay unit (that of a Lavoie, Model LA-265 oscilloscope) connected between the "Cossor" pulse generator (see Section 2.2.1) and the recording oscilloscope. The response of the two photomultipliers to a particular current pulse is shown in Fig. 3.2.6.(v)a. Here the oscilloscope was triggered some 95 μs after the discharge was initiated. The upper trace represents the light pulse at the anode end, while the lower trace represents the light pulse obtained at the cathode end. The pulses have a rise-time of about 750 μs and a width of about 2.5 μs. The peak of the anode pulse can be seen to lag that of the cathode pulse by about 100 ns. To check the nature of the delay, the two photomultipliers were interchanged, and the light pulses again observed. The results obtained are shown in Fig. 3.2.6.(v)b, where the upper and lower traces represent, as before, the anode and cathode light pulses, respectively. It can be seen that the anode pulse now appears to lead instead of lag the cathode pulse by about 100 ns. It is clear from this, that the delay is an instrumental effect, and that if the current pulses represent a wave phenomenon, they would have to propagate across the gap in less than the minimum time resolvable in the above oscillograms, i.e. in less than 100 ns. This means that the pulse must propagate at a velocity greater than 9×10^8 cm s^{-1}. This is about two to three orders of magnitude in excess of the velocities of ionization waves of the type observed by Doran (1968) - (see Section 1.1),

Fig. 3.2.6.(v)a Oscillogram showing photomultiplier traces of light pulses detected at the anode end (upper trace) and cathode end (lower trace), 5 cm from either electrode of the metre-chamber, for a 0.80 Torr SF_6 spark pulsed at 12.00 kV.

Fig. 3.2.6.(v)b Oscillogram showing the same traces shown in Fig. 3.2.6.(v)a, but with the photomultipliers interchanged.

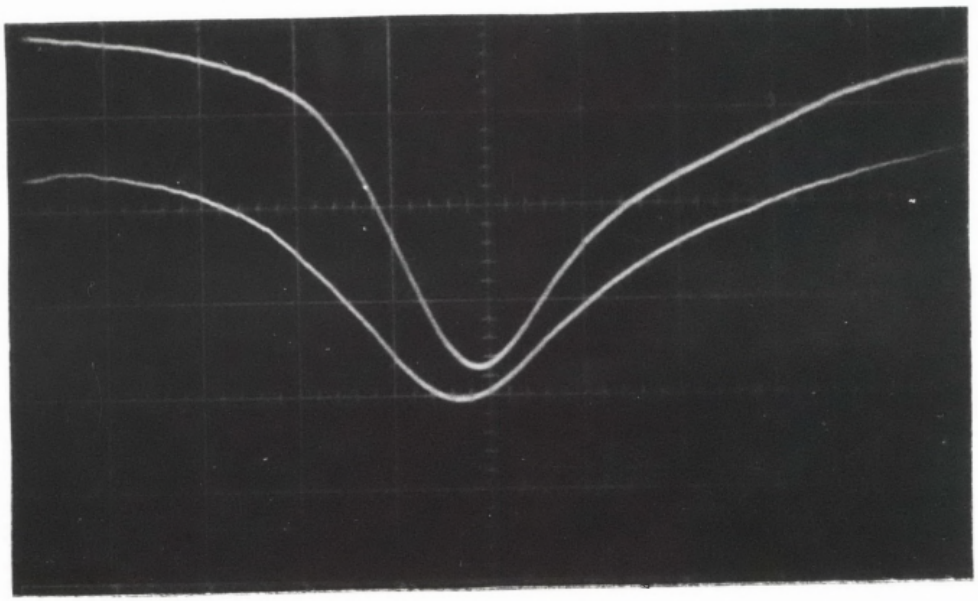

Time (500ns/div.)

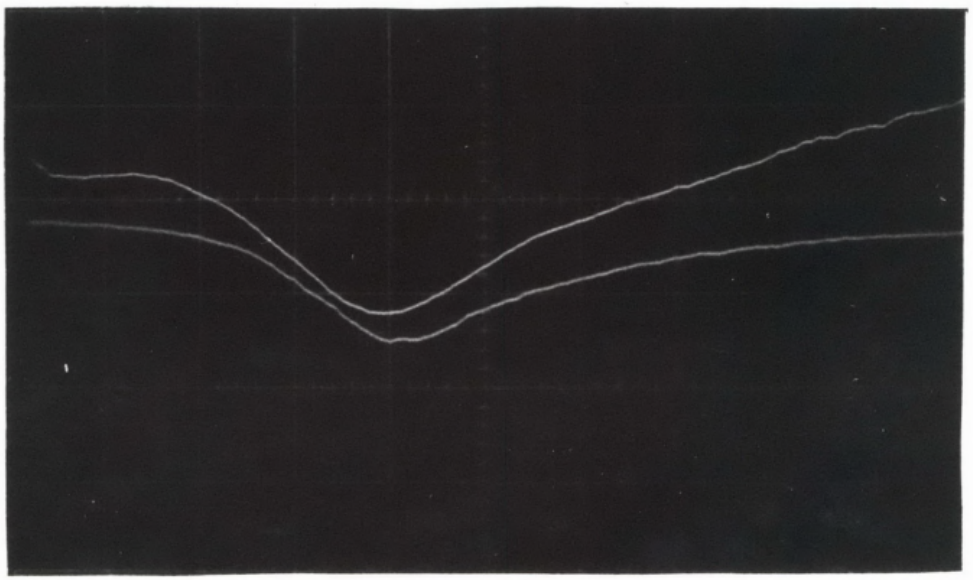

Time (500ns/div.)

and about six to seven orders of magnitude greater than the velocities of moving striations observed in electronegative gases at low pressures (Woolsey *et al.*, 1965).

When the photomultiplier method was likewise used in the search for longitudinal wave propagation in the d.c. SF_6 discharge, only an instrumental delay between the light pulses was evident, as in the SF_6 spark.

A final check for axial wave propagation was made by using the capacitative probe method of Ishikawa and Suganomata (*loc. cit.*), in a 0.5 Torr d.c. SF_6 glow discharge maintained at 3 mA. These discharge conditions are similar to those used by the above workers (0.05 Torr $\leqslant p \leqslant$ 0.6 Torr, and 0.1 mA $\leqslant I \leqslant$ 2 mA). The recording oscilloscope was internally triggered by the voltage pulse induced in one probe fixed close to the anode, and the phase difference between this pulse and the voltage signal induced in a second probe, was examined as the second probe was moved over the full length of the discharge tube. Using a time-scale of 500 ns per division, no phase change was observed to within 50 ns. Waves with the velocities reported by Ishikawa *et al.* would have been easily resolvable on this time-scale. An increase in the amplitude of the probe signal was presently found to occur from anode to cathode, as observed by Ishikawa *et al.*, when the circuitry was arranged as in their experiment, with the cathode at a high negative potential and the anode grounded. Ishikawa *et al.* interpreted this as an increase in the wave amplitude as it propagated from anode to cathode. However, it was presently observed that if the reverse arrangement was used, with the anode at a high positive potential and cathode grounded, the probe signal became smaller closer to the cathode. This suggests that these changes in amplitude of the probe signal may be a circuit effect.

On the basis of the photomultiplier and capacitative probe findings, it appears that the current pulse phenomenon is unlikely to be a wave propagating axially along the discharge tube.

(b) *Radial propagation*

Radially propagating ionization waves have been suggested to occur in some gas discharges (Kiselevskii and Suzdalov, 1974 - see Garscadden, 1978), and so some attempts have been made to check the possibility of such a phenomenon in the present SF_6 discharges. For these investigations, the metre spark-discharge was used (p = 0.8 Torr, $V_{applied}$ = 12.00 kV) and the recording oscilloscope externally triggered as earlier explained. The two photomultipliers and their aperture-housings were set at right angles to the discharge tube and arranged so as to observe light pulses at different radial positions. A delay between the two pulses was observed, but was always found to be instrumental to within 50 ns, upon interchanging the photomultiplier leads. A second experiment was performed in which the p.m. tubes were used to observe simultaneously, the light pulses at any two radial positions, by looking down the discharge end. Although optical arrangements were set up to observe light pulses from specific cylindrical shells, the results obtained were complicated by end-effects near the ring-electrodes.

An independent technique in the search for possible radial waves was attempted, in which the current pulses rather than light pulses were examined. The conventional ring anode was replaced by a planar stainless-steel "multiple-ring" anode, which consists of a small central disc surrounded by six closely spaced concentric annular rings. These components were held in position and electrically isolated from one another by an "Araldite"-based compound. A phase difference was looked for between current pulses recorded at different annular rings, assuming that if any radial motion occurred along the length of the positive column, it would also occur at the anode surface. A finite delay was observed between current pulses monitored at the central disc collector (of mean radius, 1 mm) and the sixth annular ring (of thickness 1 mm and mean radius, 12 mm). However, this delay was also shown to be instrumental to within 50 ns. Hence, any radial wave propagation would have to occur, if at all, at a velocity in excess of 2.5×10^7 cm s^{-1}.

3.2.6.II(iv) An investigation of the role of the electrodes and the electrode gap

It is known that anode and cathode instabilities are capable of generating oscillations in gas discharges (Gray *et al.*, 1966). To check whether the observed current pulses may be related to such instabilities, a 2.5 Torr d.c. SF_6 discharge was maintained in the variable-gap chamber after freshly cleaning and polishing the electrodes. A photomultiplier was used to examine the light pulses corresponding to the current pulses, at different axial positions within the gap and especially at the two electrodes. It was observed that the light pulses had a constant intensity at all axial positions from anode to cathode. This suggests that the current pulses are not due to electrode instabilities such as anode or cathode spots, since oscillations due to such instabilities are generally observed to grow in amplitude closer to the instability. By maintaining the d.c. discharge for several minutes, anode and cathode spots could be obtained. An examination of these with the photomultiplier showed light oscillations of frequencies much higher than those of the current pulses. These oscillations were observed to decrease rapidly in light intensity beyond a few mm. from the luminous spots, while the light pulses associated with the current pulses remained at the same amplitude for all axial positions. These observations suggest that the current pulses are not related to electrode effects.

Information on the origin of the current pulses was obtained by varying the electrode separation. As the electrode separation is reduced, while maintaining constant the pressure and the base-current, the amplitude of the pulses decreases and the frequency increases. For a 0.5 Torr, d.c. SF_6 discharge maintained at a base-current of 2 mA, it was observed that when the electrode separation was reduced to a value where the discharge no longer possessed a positive column (this separation being 2 cm for the above pressure and base-current conditions), the current pulses suddenly disappeared.

The lack of control exerted on the pulses by the electrodes, together with the need for a positive column to exist if the pulses are to occur, clearly suggests that discharge processes in the positive column are responsible for the current pulse phenomenon. Furthermore, the apparent lack of any propagating wave, as indicated by the results of II(iii), suggests that the pulse-generating processes may take place simultaneously over the length of the column. In order to gain further insight into the pulse-generating mechanism, a series of investigations was made into some of the fundamental properties of the positive column in the low pressure SF_6 glow discharge.

3.2.6.II(v) An investigation of the positive column

(a) *E/N and the mean electron energy at pulse onset in the d.c. and spark discharges*

In II(ii), it is seen that the onset of current pulses appears to be governed by a critical discharge voltage. In view of the results of II(iv) regarding control by the positive column, an investigation was made to see if this critical voltage translated into a critical value of E/N for the column. Results of measurements made for different combinations of pressure and base-current, under both d.c. and spark conditions, do in fact point to a critical E/N and hence a critical mean electron energy being attained just before the production of a current pulse.

From the voltage oscillogram of Fig. 3.2.6.(i)a (which as indicated earlier, refers to a 0.8 Torr d.c. SF_6 discharge maintained in the metre-chamber at a base-current of 3 mA), the voltage across the metre-gap immediately prior to pulse-onset is 9.6 kV, so that the column field (E) at that time is approximately 86 Vcm^{-1}, assuming a cathode fall of 1 kV on the basis of values obtained in the spark work under similar discharge conditions. The gas number density (N) in the column of the above d.c. discharge has been measured using the Lee-Woolsey interferometer. With the scene-beam located on the tube axis, the discharge was suddenly switched-off, and a fractional fringe shift of almost exactly one-half was measured in the direction corresponding to increasing number density. Using equation 2.3.2e, the gas number density in the column

is thus evaluated to be 1.55 x 10^{16} cm^{-3}. Hence the column E/N-value at pulse onset is calculated to be 555 Td, at which the mean electron energy is 12.0 eV, as evaluated, referring to the D/μ-data of Fig. 1.3.3.(iv) and assuming a Maxwellian electron energy distribution in equation 1.3.3v. (The assumption of a Maxwellian distribution is likely to be reasonable for a glow discharge positive column. If Kline *et al.*'s (1979) computed electron energy distribution is assumed (see Section 1.3.3.(iv)), the mean electron energy is 10.5 eV at 555 Td.).

Very similar values of mean electron energy at pulse onset to that obtained in the d.c. metre-discharge above, have been measured in d.c. discharges in the movable-electrode chamber under varying conditions of pressure and base-current. The threshold column fields in the movable-electrode chamber, have been determined by measuring the gap voltage at pulse onset at different electrode separations, under conditions of constant discharge base-current. Due to the nature of the chamber design however, it has not been possible to measure the gas densities in the movable-electrode chamber using the Lee-Woolsey interferometer. A thin chromel-alumel thermocouple of wire diameter 0.12 mm has thus been used to determine the gas number density in the discharge column from measurements of the gas temperature in the discharge. The thermocouple unit is inserted into the movable-electrode chamber through the vertical side-arm shown in Fig. 2.1.1, using an 'O'-ring coupling arrangement. The gas temperatures measured in the small tube with the thermocouple have been remarkably consistent, for any particular combination of discharge pressure and base-current, with those deduced from gas density measurements obtained with the Lee-Woolsey interferometer in the metre-gap, for the same low pressure and low current d.c. discharge conditions. This consistency suggests that heat losses at the thermocouple surface under the present discharge conditions can be neglected. The ideal gas law has been used assuming constant gas pressure, in determining the discharge gas density in the movable-electrode chamber from the temperature measurements. The column fields at pulse onset are shown in Fig. 3.2.6.(vi) for three combinations of pressure and base-current. The discharge gas temperatures measured during these field measurements varied from 452 K to 605 K,

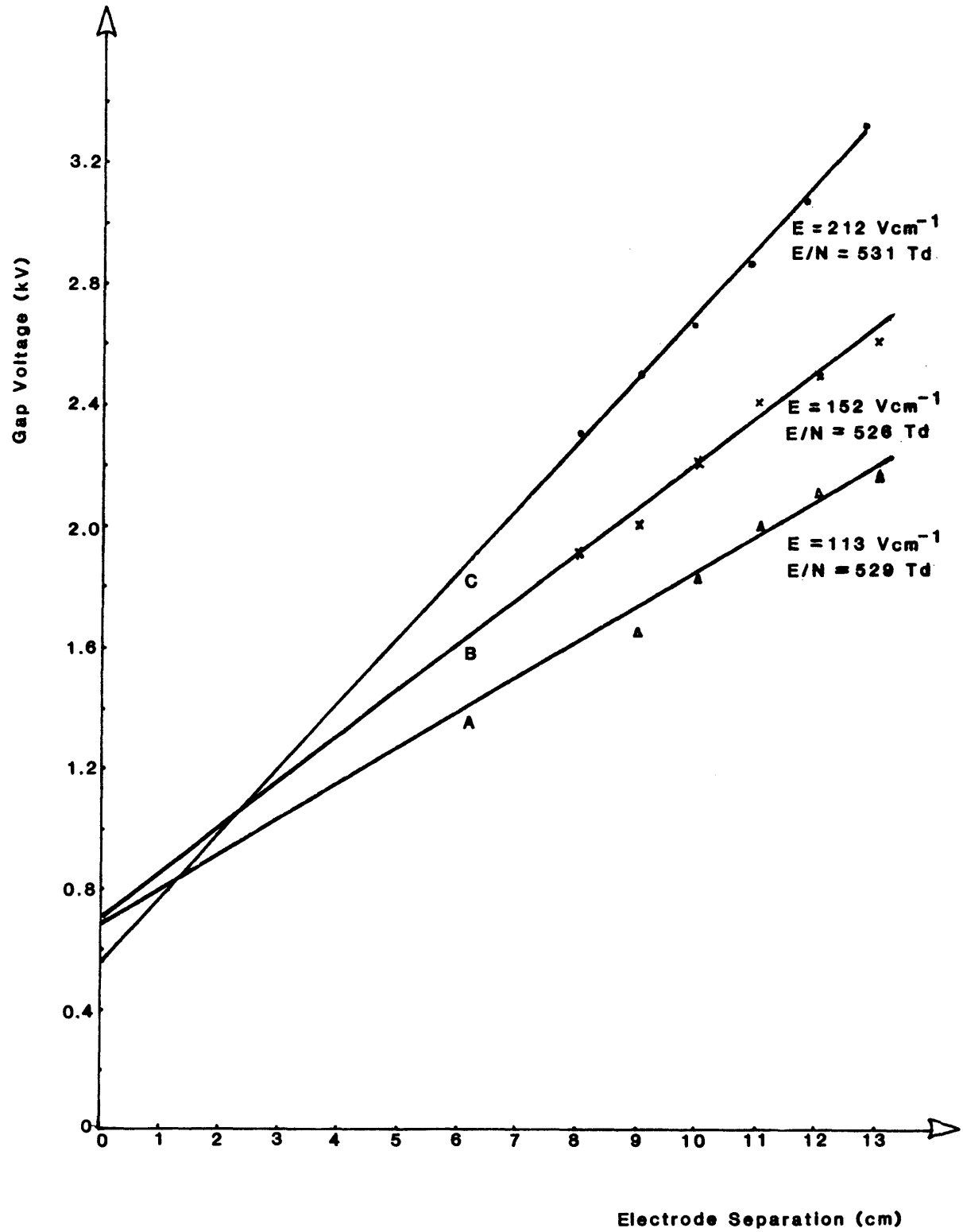

Fig. 3.2.6.(vi) Axial voltage distributions at pulse-onset in the d.c. SF_6 discharge for three separate combinations of gas pressure, base-current and axial gas temperature.
Curve A: p = 1.0 Torr, base-current = 2.5 mA, T = 452 K;
Curve B: p = 1.5 Torr, base-current = 3.0 mA, T = 501 K;
Curve C: p = 2.5 Torr, base-current = 4.0 mA, T = 605 K.
The calculated E/N values at pulse-onset are also shown for each of the curves.

but remained constant for a particular combination of pressure and base-current, to within 2%, during an entire experimental run. These temperatures are indicated in the above figure. It can be seen that the E/N-values obtained at pulse onset for the three sets of discharge conditions are effectively constant and give an average value of 529 ± 3 Td. Again assuming a Maxwellian distribution, the mean electron energy corresponding to this E/N-value is 11.8 eV. This mean electron energy lies within 2% of the value obtained in the metre-chamber (for a base-current of 3 mA and pressure of 0.8 Torr).

The axial E/N-value in the 0.8 Torr, 12 kV spark discharge pulsed in the metre-gap (refer to Fig. 3.2.2.(iv)a), has been estimated to be approximately 400 Td at the onset of the pulses found in the early stages of the electronegative glow phase. The column field in this spark has been estimated from the voltage oscillogram of Fig. 3.2.2.(iv)a, assuming a cathode fall of 1 kV, while the gas density is known from the Lee-Woolsey measurements to have decreased negligibly from the initial value, at these times. The mean electron energy thus obtained assuming a Maxwellian distribution, and using the electron characteristic energy (D/μ) results of Kline *et al.*, is 10.5 eV.

These results suggest that the onset of the current pulses in the positive column is associated with a critical value of E/N which in turn implies a critical value of mean electron energy. The discrepancy between the values of E/N measured in the spark and d.c. discharges may be due to a difference in the electron energy distributions in the two forms of discharge. That is, it is possible that the onset of a current pulse does occur at the same mean electron energy in all cases.

(b) *A spectroscopic investigation of the d.c. discharge*

A spectroscopic analysis was performed of the low current and pressure d.c. SF_6 glow discharge, using a half-metre, Ebert scanning spectrometer (Jarrell-Ash, Model 82-025) in conjunction with one or other of the photomultipliers described earlier in II(iii)a. The spectrometer, with a grating blazed for 5000 Å, has the capability of scanning from 1900 Å to 9100 Å. The spectrometer was set up so as to view the d.c. discharge in the movable-electrode

chamber, through a fused silica window attached to the vertical side-arm shown in Fig. 2.1.1. It was observed that during the interpulse regime, the column radiation is dominated by atomic fluorine lines (such as 685.6 nm, 690.2 nm, 624.0 nm, 704.4 nm, etc.). Interestingly, it was observed however, that the light pulses themselves are dominated not by the SF_6 discharge spectrum but by the second positive band system of nitrogen ($C^3\Pi_u - B^3\Pi_g$). The most intense band heads observed were at 337.1 nm, 315.9 nm and 357.7 nm, although other band heads at 380.5 nm, 375.5 nm and 311.7 nm were also of appreciable intensity (a complete list of band spectra in this nitrogen system is given by Pearse and Gaydon, 1976). None of the intense wavelengths observed could be attributed to the other air impurities such as oxygen or water vapour.

(c) *The measurement of the negative ion-to-electron number density ratio (β) in the positive column*

Section 3.2.6.I shows that the electronegative glow phase is dominated by negative ions, and, as will be seen, these negative ions play a significant role in the generation of the current pulses in the positive column. As an aid to the interpretation of the pulse-generating mechanism, a Langmuir probe analysis was made of the d.c. positive column in order to obtain data on electron and negative ion densities. The Langmuir probe technique is one which is much more readily applied to d.c. discharges than to pulsed discharges.

A cylindrical tungsten probe of diameter 0.3 mm and length 3 mm was built and inserted into the movable-electrode chamber through the vertical side-arm. Using an 'O'-ring arrangement, the probe could be moved across the diameter of the discharge tube. The probe was grounded through a 10 kΩ resistor, and probe potential V_p relative to plasma potential was altered by applying to the anode a variable potential relative to ground, with the cathode potential floating. Probe current-voltage characteristics could then be obtained by applying this variable potential to the X input of an XY recorder while the voltage across the probe resistor was applied to the Y input, the latter giving a measure of the probe current (i_p).

The d.c. SF_6 discharge was maintained in the very low-current, diffuse and pulseless phase, since the probe characteristics obtained in the constricted (pulse) regime were too noisy to allow detailed analysis. Typical probe characteristics are shown in Fig. 3.2.6.(vii). These were obtained 8 mm from the anode, on the axis of a 2.5 Torr, d.c. SF_6 discharge maintained at 0.35 mA and 0.8 mA. The nearly symmetrical nature of the characteristics to either side of floating potential V_f (at which zero net probe current is obtained), indicates a very small influence of the electrons on the probe currents. This is typical of highly electronegative plasmas (Woolsey *et al.*, 1973). Although careful inspection of the characteristics reveals that the total negative probe current exceeds the positive current at any absolute value of V_p (with respect to V_f), the difference between these is always less than 10%. On account of this degree of symmetry, V_f is likely to be within a fraction of a volt of plasma (or space) potential V_s.

The analysis of the probe characteristics requires knowledge as to whether the probe currents are "orbital" or "space-charge" limited (Langmuir and Mott-Smith, 1924). Application of the orbital-limited theory requires that the Debye length λ_D be of the order of the probe radius r_p, while the space-charge limited theory is valid when $r_p \gg \lambda_D$. For the present investigations, the ion Debye length has been used in view of the fact that there are very many more ions (positive and negative) than electrons, so that the former will have greater control on the space-charge sheaths than the electrons. The ion Debye length can be taken as

$$\lambda_D = \left[\frac{2kT_{\pm}\varepsilon_0}{n_{\pm}e^2}\right]^{\frac{1}{2}} \qquad (3.2.6a),$$

where $T_{\pm}$ and $n_{\pm}$ are the positive (or negative) ion temperature and number density, respectively, k is the Boltzmann constant, e the electronic charge, and ε_0 the permittivity of free space. The ion temperature is taken to be approximately the same as the gas temperature (around 400 K). An upper limit for λ_D can be

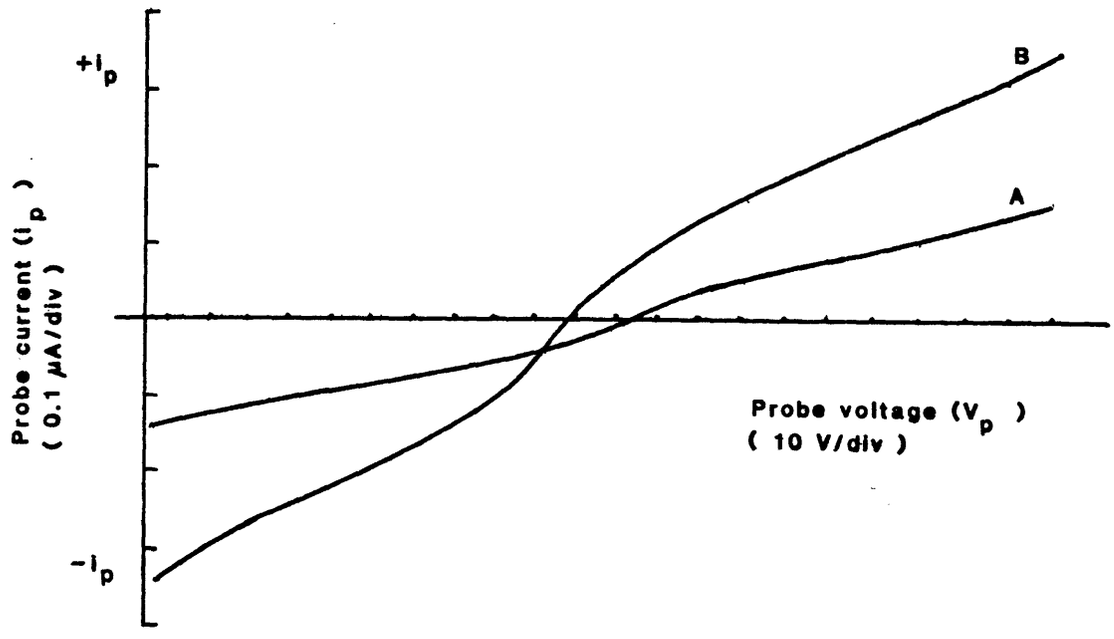

Fig. 3.2.6.(vii) Probe characteristics for a cylindrical probe located on the axis of a 2.5 Torr d.c. SF_6 discharge, and 8 mm from the anode. Curve A refers to a 0.35 mA discharge and curve B, to a 0.8 mA discharge. Both curves have been obtained in the absence of the current pulses.

calculated by estimating the electron number density n_e from the equation, $J = n_e e v_e$ and by taking $\beta = \frac{n_\pm}{n_e} = 10^2$ (the symmetry of the probe characteristics indicate that β is in fact substantially greater than 10^2). For the low currents ($\sim$ 1 mA) and the low E/N-values ($\sim$ 450 Td) in the present pulseless discharges, n_e is of the order of 10^{14} m^{-3}. The upper limit for the ion Debye length is thus calculated to be of the order of 10^{-2} mm. Hence $r_p >> \lambda_D$, which suggests that the space-charge limited analysis is the appropriate one for the present circumstances. Further justification for the use of the latter analysis has been obtained by plotting $(i_p)^2$ vs. V_p. This curve is linear for orbital-limited current collection by a cylindrical probe. Non-linear curves are obtained however, for the present discharges, as shown for example, in Fig. 3.2.6.(viii). This plot refers to a 2.5 Torr, 1 mA d.c. SF_6 discharge, with the probe located on axis and 8 mm from the anode.

It can be shown from the space-charge limited theory that $\beta = \frac{n_-}{n_e}$, is given in terms of the ratio of negative ion-to-electron probe current $\left[\frac{i_-}{i_e}\right]_p$, where both currents are measured at the same probe potential. This relationship is given by

$$\beta = \frac{n_-}{n_e} = \left[\frac{i_-}{i_e}\right]_p \cdot \left[\frac{T_e}{T_-} \cdot \frac{m_-}{m_e}\right]^{\frac{1}{2}} \qquad (3.2.6b).$$

Here T_e is the electron temperature and m_e and m_-, the electron and negative ion masses, respectively. The probe characteristics can be used to determine $\left[\frac{i_-}{i_e}\right]_p$ at any positive value of V_p, by a careful comparison of the total positive and negative probe currents. This is done assuming that zero probe current is collected at plasma potential (i.e. $V_f = V_s$, as discussed earlier) and that the negative ion probe current, $(i_-)_p$ at +V relative to V_s, is the same as the total positive probe current, $(i_+)_p$ at -V relative to V_s, allowing for a mass factor, discussed below. It is assumed here that $n_e << n_-, n_+$ and that $n_+ \doteq n_-$. The electron probe current, $(i_e)_p$ at +V relative to V_s is then given by $\left[(i_{T_-})_p - (i_+)_p\right]$, where $(i_{T_-})_p$ is the total negative probe current.

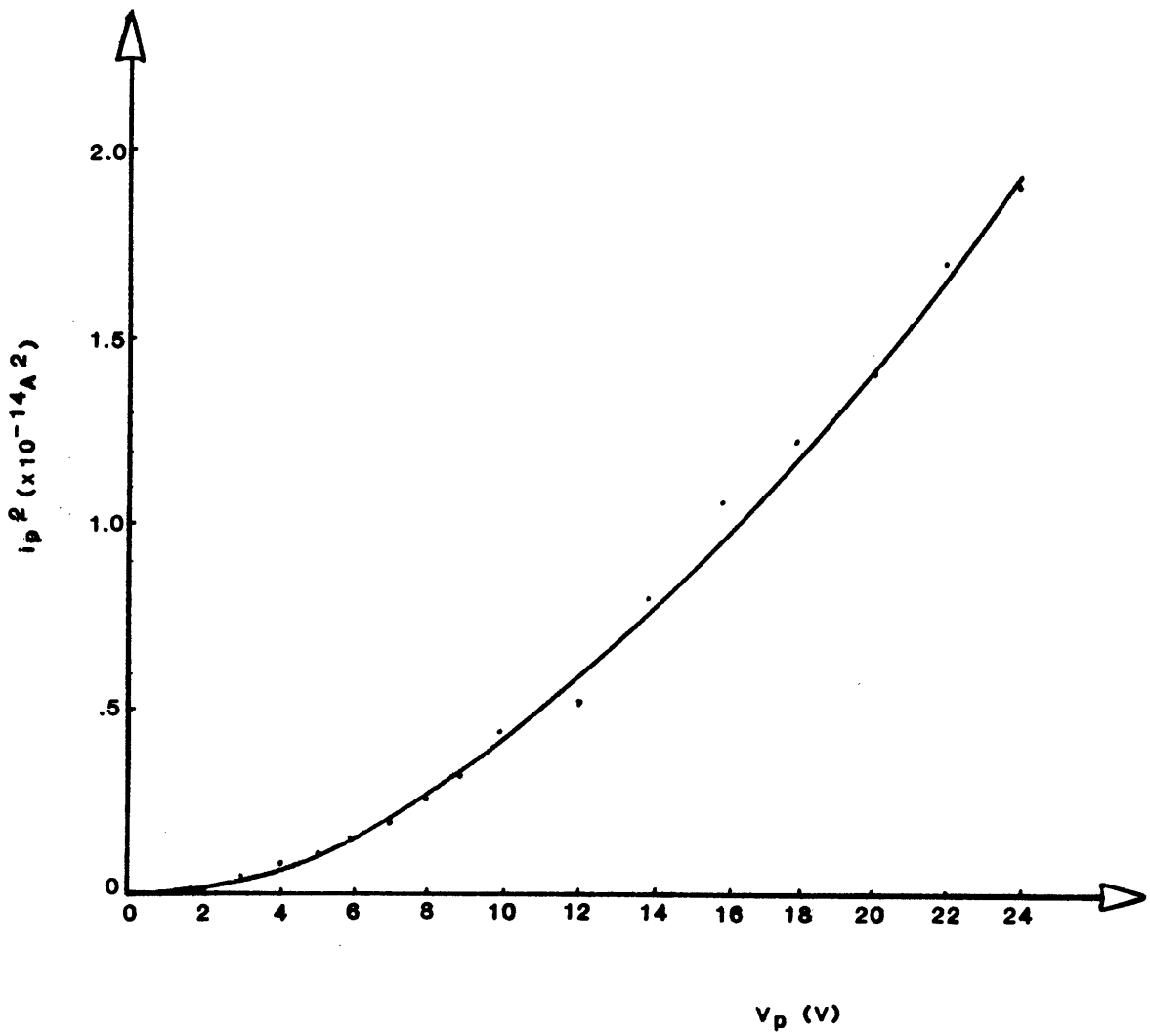

Fig. 3.2.6.(viii) A plot of $(i_p)^2$ vs. V_p, for a 2.5 Torr d.c. SF_6 discharge maintained at 1 mA, with the cylindrical probe located on the tube axis and 8 mm from the anode.

A correction factor has been introduced in the present analysis, to account for the effect of the mass difference between the dominant positive and negative ion species, on $(i_-)_p$ and $(i_e)_p$. It has been assumed that at the low discharge pressures, currents and temperatures operated at in the present probe work (2.5 Torr, $\sim$ 1 mA and $\sim$ 400 K respectively), the dominant negative and positive ion species are SF_6^- and SF_5^+ (refer to Section 1.3). Taking $n_+ \doteqdot n_-$ and $T_+ = T_-$, the negative ion current at +V relative to V_s and the positive ion current at -V relative to V_s, are in the ratio

$$\left[\frac{i_-}{i_+}\right]_p = \left[\frac{m_+}{m_-}\right]^{\frac{1}{2}} = \left[\frac{127}{146}\right]^{\frac{1}{2}} = 0.93 \qquad (3.2.6c).$$

Thus taking $(i_-)_p = 0.93(i_+)_p$, $(i_e)_p$ is given by

$$\left[(i_e)_p = (i_{T_-})_p - 0.93(i_+)_p\right] \qquad (3.2.6d),$$

where as before $(i_{T_-})_p$ is the total negative probe current at +V relative to V_s. A knowledge of $\left[\frac{i_-}{i_e}\right]_p$ thus allows β to be calculated provided the other quantities in equation 3.2.6b are known.

Measurements of probe currents, at $\pm$V relative to V_s, were made by measuring the potential difference across the probe resistor with a digital meter. For probe voltages of $\pm$40 V, positive and negative probe currents, and hence values of $\left[\frac{i_-}{i_e}\right]_p$, have been determined for a point 1 cm from the anode on the axis of a 2.5 Torr, diffuse d.c. SF_6 discharge, maintained at various currents ranging between 0.25 mA and 1.5 mA. The mean electron density was estimated using the equation

$$n_e = \frac{I}{Ae v_e} \qquad (3.2.6e),$$

where I is the total discharge current, A the cross-sectional area of the discharge tube, and v_e the electron drift velocity. An estimate for v_e at the low E/N-values operated at ($\sim$ 400 Td.) was obtained from the results of Kline *et al.*, (1979) - see Fig. 1.3.3.(iii). The negative ion temperature, T_-, has been assumed to be of the order of 400 K for the above range of discharge currents, and the electron temperature T_e has been taken to be of the

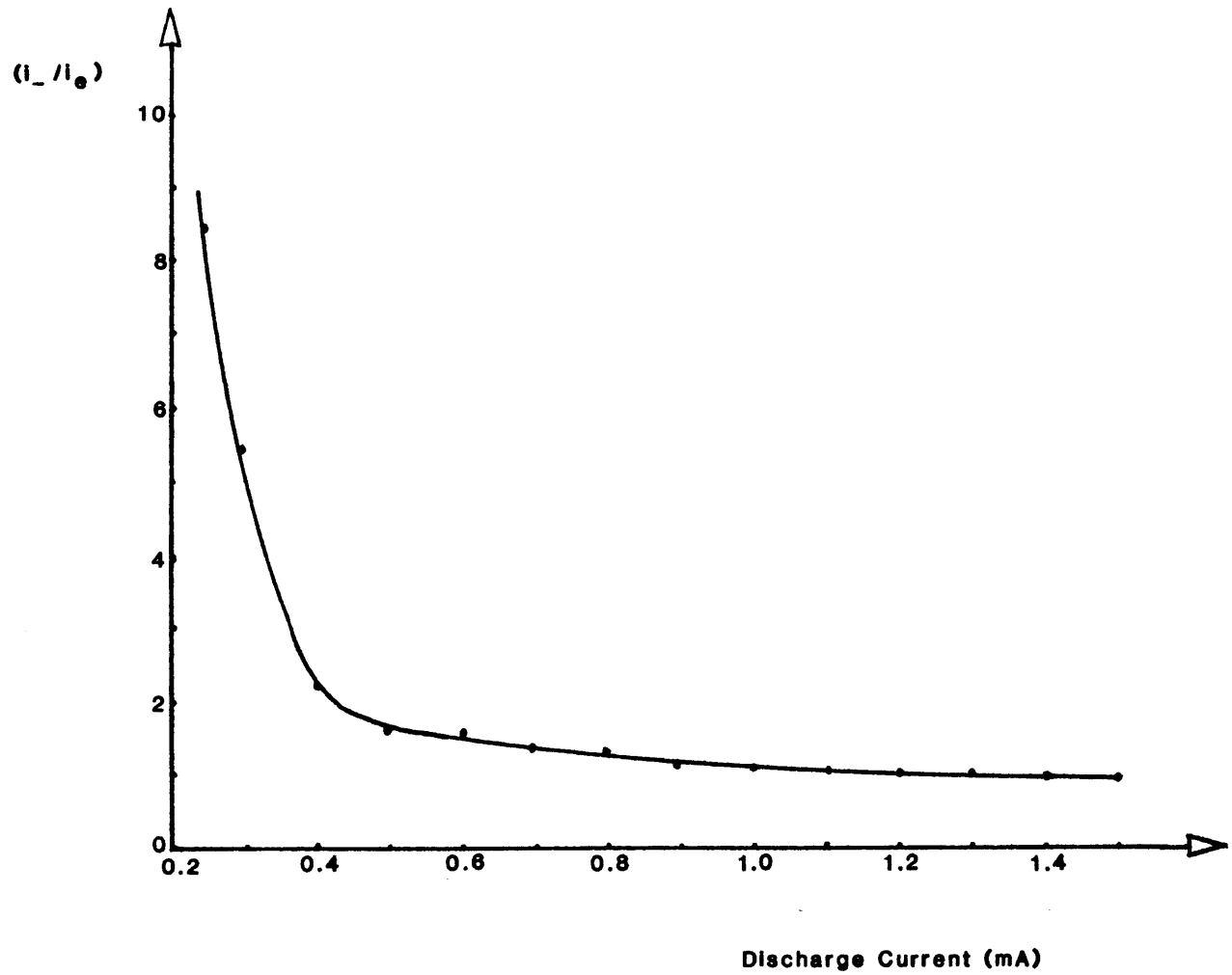

Fig. 3.2.6.(ix)a Graph of (i_-/i_e) vs. discharge current for the very low current (pulseless) regime of a 2.5 Torr d.c. SF_6 discharge maintained in a 7.75 cm gap. The (i_-/i_e) values have been determined from the appropriate probe characteristic, at a probe voltage of $\pm$ 40 V relative to V_s. For these measurements, the cylindrical probe was located on the tube axis, 1 cm from the anode.

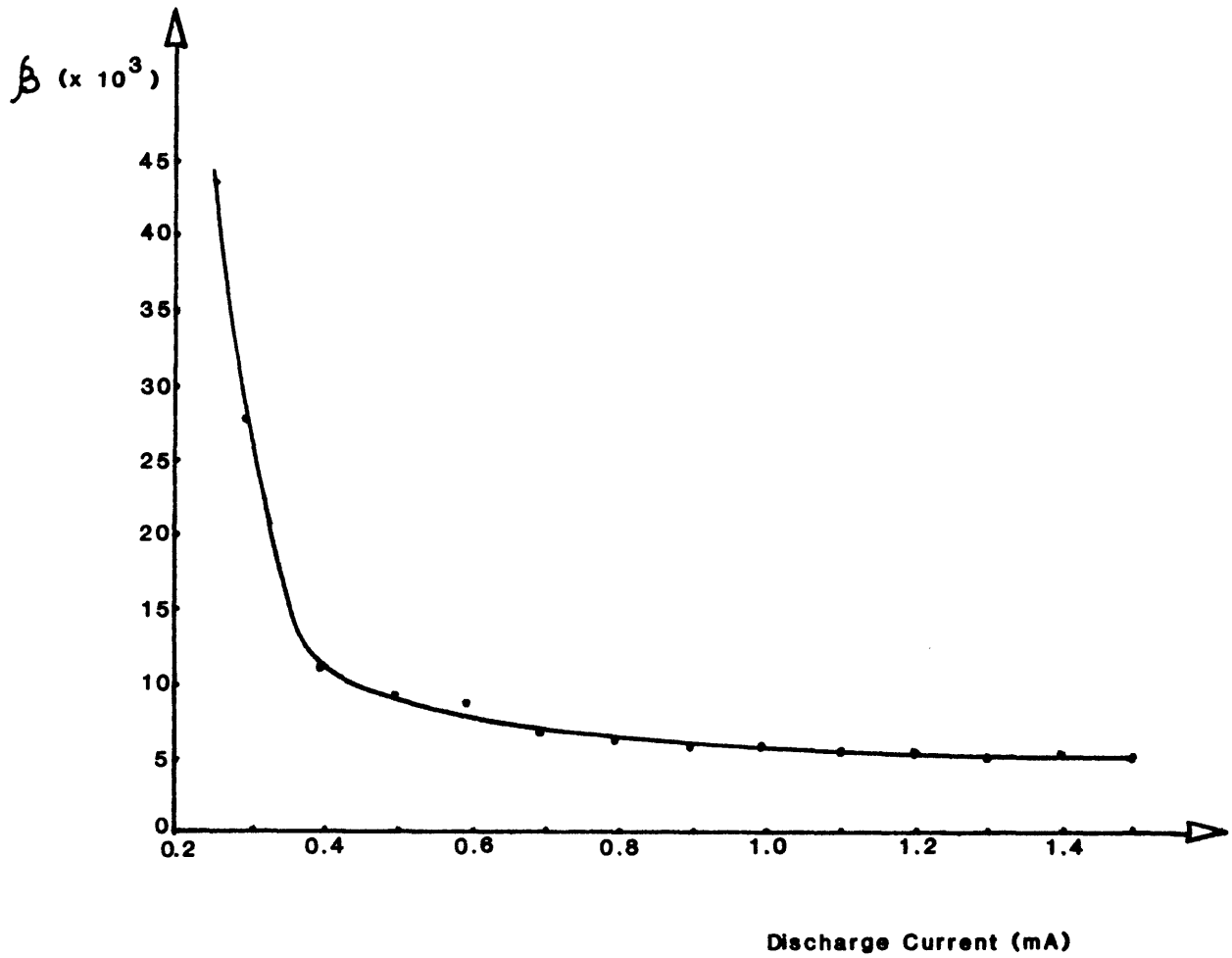

Fig. 3.2.6.(ix)b Graph of the negative ion-to-electron number density ratio (β) vs. discharge current, derived from the (i_-/i_e) data of Fig. 3.2.6.(ix)a.

order of 5 x 10^4 K, which is a value typical of electron temperatures in low pressure and low current glow discharges (von Engel, 1965). From measured values of $\left[\frac{i_-}{i_e}\right]_p$ shown in Fig. 3.2.6.(ix)a, β-values have been calculated using equation 3.2.6b, over the range of discharge current specified above. The results are shown in Fig. 3.2.6.(ix)b. At the upper limit of discharge current shown (1.5 mA), beyond which the d.c. probe measurements were not analysed due to the onset of the current pulses, β is 5 x 10^3. β rises gradually to 10^4 as the current is decreased to 0.4 mA. With further decrease below 0.4 mA, β rises more sharply, as the discharge column tends to a positive ion-negative ion plasma (Woolsey *et al.*, 1973).

3.2.6.II(vi) Discussion and conclusion

The experimental results of the foregoing sections suggest that the mechanism of current pulse generation in the low pressure SF_6 glow discharge is a positive column effect, which takes place at a critical mean electron energy. This implies either the sudden introduction of a new and efficient electron production process throughout the positive column, or a sudden decrease in some electron loss process. The responsible process must have a threshold energy. Evidence as to the nature of the pulse-generating mechanism is provided by the spectroscopic data of II(v)b, which reveals the sudden onset of excitation of the nitrogen second positive system when a current pulse is generated. The threshold energy for this excitation is 11.0 eV (Imami and Borst, 1974), which corresponds closely to the values of mean electron energy estimated from E/N measurements at pulse onset (see II(v)a), under both d.c. and spark conditions.

On the basis of this evidence, it appears that the current pulses may be the result of electron production by photodetachment of negative ions caused by u.v. radiation from the nitrogen of air impurity in the SF_6 discharge. A possible sequence of processes leading to photodetachment in a mixture of SF_6 and nitrogen is as follows:

$$N_2\ (X^1\Sigma_g^+) + e\ (\sim 11ev) \rightarrow N_2^*\ (C^3\Pi_u) + e \qquad (3.2.6f),$$

$$N_2^*\ (C^3\Pi_u) \rightarrow N_2^*\ (B^3\Pi_g) + h\upsilon\ (\sim 3.7eV) \qquad (3.2.6g),$$

$$SF_6^- + h\nu \rightarrow SF_6 + e$$

and $$SF_5^- + h\nu \rightarrow SF_5 + e \qquad (3.2.6h).$$

$$F^- + h\nu \rightarrow F + e$$

Although photodetachment cross-section data for SF_6^- and SF_5^- are not available, it could be expected that considerable photodetachment from these species might occur, since it is likely that the threshold energies for this process will be considerably lower than the maximum vertical detachment energies deduced in Section 1.3.3.(iii). The F^- concentration is likely to start becoming important at the relatively high E/N-values at pulse onset and at the moderate gas temperatures measured ($\sim$ 500-600 K) - (see Sections 1.3.3.(ii) and (iii)). Photodetachment from the F^- might thus be expected, since a finite photodetachment cross-section for this species exists at the photon energies corresponding to the most intense nitrogen wavelengths presently observed. For example, at the photon energy corresponding to the 337.1 nm wavelength (i.e. 3.7 eV) the photodetachment cross-section is of the order of 4×10^{-18} cm^2, as shown in Fig. 1.3.3.(ii). The photodetachment threshold (equal to the electron affinity in the case of atomic fluorine) is 3.4 eV.

Further evidence to support this photodetachment mechanism has been provided by recent experiments in a new discharge tube and vacuum system, in which it has been possible to substantially reduce the impurity levels. D.c. SF_6 glow discharges, under similar conditions of pressure, current and gap length to those already described, can be maintained in this system without the existence of current pulses. The system consists of a small glass discharge chamber with a fixed gap of 8 cm which is free of ground-glass joints and which is connected via a glass-to-metal seal to an all-metal vacuum system. It uses copper-sealed "Conflat" flanges rather than ordinary 'O'-ring seals. The vacuum system has an apparent leak-rate of about 0.1 mTorr per hour after adequate pumping and out-gassing.

Further preliminary experiments with the new discharge tube and vacuum system indicate that current pulses occur in the low pressure SF_6 glow discharge

when the air impurity rises above about 1 part in 10^4 of SF_6. In the discharge systems used for most of the present work, the leak-rates of arount 5 mTorr per hour are likely therefore to provide enough nitrogen to generate the current pulses through the photodetachment process.

Additional evidence is available in support of the proposed photodetachment mechanism from the results obtained on the variation of current pulse amplitude with added capacitance across the discharge gap, and from probe measurements of negative ion-to-electron number density ratios (β-values). As indicated in Section II(ii)b, and illustrated in Fig. 3.2.6(iv), the current pulse amplitude increases with added capacitance and saturates at a value of the order of 10^3 times the base-current. For the discharge conditions shown in Fig. 3.2.6.(iv) (i.e. for p = 2.5 Torr, d = 11 cm, base-current = 3 mA), a careful observation of the gap voltage has revealed that the rate at which the latter collapses during a current-pulse, decreases with increasing added capacitance. Thus for no added capacitance, a collapse of 370 volts occurs in approximately 400 ns, giving a decay rate of approximately 0.92 V ns^{-1}. As the capacitance is increased, the gap voltage collapses by a smaller amount during a current pulse and takes longer to decay. Thus for the 30000 pF capacitor, the voltage collapses by only 140 volts and decays in 1800 ns, giving a decay rate of 0.08 V ns^{-1}, This is a decrease of over 90% in the decay rate, and obviously indicates that as larger capacitance values are added across the discharge tube, the gap voltage is maintained closer to the pulse-onset value for much longer. If photodetachment occurs, the mean electron energy will thus be held close to the threshold value for longer times, and this would allow many more negative ions to become photodetached by the nitrogen radiation. The saturation pulse amplitude suggests that there comes a stage where a maximum number of negative ions in the discharge becomes photodetached and where maintaining the gap voltage close to the photodetachment threshold for longer times has no further effect.

The value of 10^3 for the ratio of saturation pulse amplitude to base-current suggests therefore that the negative ion-to-electron density ratio (β) in the inter-pulse phase must be of this order of magnitude. This correlates quite well with the results of the Langmuir probe analysis in Section II(v)c, where β-values of the order of 10^3 were measured. The probe measurements were of course made in the absence of current pulses, but at the higher discharge currents ($\sim$ 1.5 mA) considered in the latter measurements, conditions are likely to be somewhat similar to those existing in the interpulse phase of a 3 mA discharge containing pulses.

Among other mechanisms that may be considered as being responsible for the current pulses, is a sudden increase in ionization. A sudden increase in electron-impact ionization requires a sudden increase in E/N, which does not occur. The onset of two-stage ionization is a possibility, although no appropriate mechanism is known to have a threshold around 11 eV in the SF_6/N_2 system. Another possible mechanism is a sudden decrease in the rate of electron loss. In the low current SF_6 positive column, electron loss occurs mainly through attachment. A decrease in the attachment rate requires either a sudden increase in mean electron energy or a sudden decrease in neutral SF_6 concentration. The results of the measurements of E and N show however that neither of these occurs at the onset of a current pulse.

The results and analysis described here indicate the important part that can be played by an impurity in the behaviour of SF_6 spark and d.c. discharges. Obviously, there is much scope for further work on this current pulse phenomenon. On the experimental side, the effect of controlled addition of nitrogen to the pure SF_6 discharges needs to be examined. On the theoretical side, the establishment of a quantitative photodetachment model is an ultimate goal. This will require a detailed knowledge of the concentration of the nitrogen impurity in the SF_6, together with cross-sections for excitation of the nitrogen second positive system, and the cross-sections for photodetachment of all the negative ion species, as a function of electron energy in SF_6/N_2 mixtures.

3.2.7 The Dissociated Glow Phase, t_D-t_E

At overvoltages below about 100%, the electronegative glow phase in the SF_6 sparks presently studied, slowly decays and no further discharge transitions are observed. Above this overvoltage however, the transition to another quasistable glow phase, termed the dissociated glow, takes place at time t_D (see Fig. 3.2.2.(ii)). At overvoltages up to about 145%, this phase lasts for a couple of milliseconds and then decays, while above this overvoltage, a transition to an arc discharge (at time t_E) is often observed, provided a low enough series resistance is used (as is done with the movable-electrode chamber).

The present section deals with the transition to the dissociated glow phase, the dissociated glow phase itself, and its subsequent decay when arcing does not occur.

3.2.7.(i) Results

(a). *Observations made from current and voltage oscillograms*

The i-t and V-t characteristics of Fig. 3.2.2.(iii) and (iv) clearly reveal the transition to the dissociated glow phase, at time t_D. The current is seen to increase, in the case of the 1.5 Torr, 9 cm spark pulsed at 3.0 kV (Fig. 3.2.2.(iii)a) from 400 mA to 1.4 A while, in the 0.8 Torr, 1 m spark pulsed at 12.00 kV, the current increases from 5 mA to about 720 mA (see Figures 3.2.4.(iii) and (iv)). From Fig. 3.2.2.(iii), the amplitude of the dissociated glow current can be seen to increase as the applied overvoltage is raised.

Other observations that are apparent from the oscillograms are the decrease in the time to the transition, as well as in the actual time of transition, with increasing overvoltage, and also the noise and current instability which suddenly appear after the current has started to increase at the transition, and which then persist throughout the dissociated glow phase.

Using the current and voltage data from each of the three sets of oscillograms of Fig. 3.2.2.(iii), calculations have been performed to determine the total energy (ε) delivered to the gap from breakdown until time t_D. This has been done using the equation

$$\varepsilon = \int_{t_A}^{t_D} Vi \, dt \qquad (3.2.7a)$$

where i and V are the instantaneous gap current and voltage respectively, and t is the time. The calculations reveal that the energy input up till time t_D for the three separate discharges represented in Fig. 3.2.2.(iii), is the same to within 5%. An average energy input of $(4.7 \pm 0.2) \times 10^{-2}$ J was obtained. The significance of this finding will be discussed in Section 3.2.7.(ii).

(b). *Interferometric measurements*

From the measurements made of changes in absolute plasma refractivity using the Lee-Woolsey interferometer, and of radial plasma refractivity gradient using the modified Jamin interferometer, useful information has been obtained regarding the discharge transition at time t_D.

Figure 3.2.4.(v) shows that the axial plasma refractivity in the 0.8 Torr, 12.00 kV SF_6 spark pulsed in the metre chamber, suddenly increases at time t_D to a value in excess of the initial refractivity. As discussed in Section 3.2.4, this suggests a sharp increase in particle density at time t_D, to a value in excess of the initial particle density. The oscillogram of Fig. 3.2.4.(iv) shows very clearly that the increase in particle density begins precisely at time t_D, and no later.

Figure 3.2.4.(ii), which shows a typical plot of the temporal variation in the radial plasma refractivity gradient in a 0.55 Torr, 10 kV SF_6 spark (pulsed in the metre-gap), indicates that there is no observable variation in the refractivity (and hence density) gradient until about 40 μs after the commencement of the current rise at time t_D. This can be more clearly seen from the Jamin interferometer trace of Fig. 3.2.4(i).

3.2.7.(ii) Discussion

A theory often used to account for current increases in many ordinary discharges, is one based on the development of a radial thermal gradient (Rogoff, 1972:- see Section 1.1 of this thesis; Marode and Bastien, 1978). The increase in axial temperature which occurs as the discharge current flows, brings about a decrease in axial gas density (N) and hence an increase in axial E/N, for constant E. The resultant increase in ionization causes further gas heating in the axial region and leads to a further rise in the axial E/N. This process is cumulative and a large current increase may thus result.

If such a mechanism is responsible for triggering the current increase presently observed in the SF_6 spark, then the radial gradient in gas density off-axis should be observed to steepen as a function of time before the onset of the main current increase. As mentioned in the previous section, this is not observed to occur until about 40 μs after t_D. The experimental uncertainty of every point of the refractivity gradient curve of Fig. 3.2.4.(ii), is $\pm$ 9.5 x 10^{-8} cm^{-1}. Using equation 3.2.4i, this implies that the average particle density gradient between the two laser beams of the Jamin interferometer (located 6 mm and 10 mm off-axis) lies within 3.3 x 10^{15} cm^{-4}, until 40 μs after time t_D. From these measurements therefore, it appears unlikely that the current-rise at time t_D is caused by an increasing radial gradient in E/N. Indeed Figures 3.2.4.(i) and (ii) suggest that it is the increase in current at time t_D which initiates a significant increase in the E/N-gradient.

On the basis of the results presented in Sections (ia) and (ib) above, it appears that an appreciable degree of dissociation of the gas starts to occur at time t_D. Support is available for this suggestion, from both calculation and experiment.

A calculation has been performed to determine the average gas temperature at time t_D, on the assumption that most of the energy delivered to the gap up till that time is used up in heating the gas molecules. This assumption is plausible on the grounds that (i) radiation energy losses are likely to be small at the low currents in the electronegative glow phase and at the low pressures operated at, and (ii) heat losses through wall-diffusion will be small since the thermal conductivity of SF_6 plasmas at temperatures below that of dissociation, is low (see Section 1.3.2.). It is likely that the gas will be heated mainly through inelastic electron-molecule collisions, in particular through the absorption of energy by the SF_6 molecules into the numerous vibrational modes of excitation. The energy absorbed by the gas up until time t_D can be written as,

$$\varepsilon = \int_{t_A}^{t_D} Vi \, dt = NA\ell C_v \Delta T \qquad (3.2.7b),$$

where N is the gas number density, A the discharge cross-sectional area, ℓ the gap length, C_v the specific heat at constant volume per SF_6 molecule, and ΔT the temperature rise in the column during time t. As mentioned earlier, the energy delivered to the gap until time t_D, for the discharges represented by the oscillograms of Fig. 3.2.2.(iii), is equal to 4.7×10^{-2} J. C_v, which is equal to 1.8×10^{-22} JK^{-1}, represents a mean value over the temperature range of interest ($300 \text{ K} \lesssim T \lesssim 2000 \text{ K}$) - (JANAF Thermochemical Data, 1965), N is taken as 4.9×10^{22} m^{-3}, ℓ is equal to 9×10^{-2} m, and A is taken as 3.8×10^{-5} m^2 (On the basis of observations made of d.c. SF_6 discharges operating at similar pressures, and at currents similar to those

of the electronegative glow phase, the discharge column of the SF_6 spark in the latter phase, is assumed to be radially contracted to a diameter of 7 mm). Assuming an initial gas temperature of 300 K, the calculation yields a gas temperature 1850 K at time t_D in the constricted discharge. This temperature is high enough for appreciable thermal dissociation to occur, on the basis of a semiempirical calculation made in Section 1.3.2 from which it was shown that the temperature for 'half-dissociation' in SF_6 is about 1250 K for a gas pressure of 1 Torr. (This latter calculation assumes that the dissociation temperatures of Frost and Liebermann (1971) at pressures of 1 Atmosphere and above, can be extrapolated to give values at low pressure.) The discrepancy between the calculated and predicted temperatures could be accounted for by finite heat loss.

Further supportive evidence has been obtained for this dissociation hypothesis by a comparison of Fig. 3.2.4.(v) with corresponding curves showing changes in axial plasma refractivity in hydrogen and argon sparks under roughly similar spark conditions. Hydrogen has been chosen because it has a dissociation energy of 4.48 eV, which is comparable with that of SF_6, and argon has been chosen because it cannot dissociate. The curves obtained for hydrogen and argon are presented in Fig. 3.2.4.(vi)b, c and d, where the SF_6 curve is included for comparison (Fig. 3.2.4.(vi)a). It can be seen that when an 8 Torr hydrogen spark is pulsed in the metre-gap at 11 kV, the curve obtained (Fig. b) is closely similar to that of SF_6, with a sharp increase in plasma refractivity and hence density, following the initial decrease. However, at lower applied voltage (7 kV) and pressure (4 Torr) the hydrogen curve (Fig. c) appears rather similar to that of a 0.8 Torr argon discharge pulsed at 4.5 kV (Fig. d), for which there is a decrease in plasma refractivity, with no subsequent sharp increase as found in Figures a and b. These results can be accounted for in terms of the existence or non-existence of thermal dissociation. It is suggested that in the high voltage case (Fig. b) for hydrogen, dissociation occurs, whereas at lower voltages (Fig. c) the hydrogen fails to dissociate.

On the basis of the above observations together with the gas temperature calculations, it is concluded that thermal dissociation of the SF_6 gas occurs at time t_D.

The primary dissociation process will be

$$SF_6 \rightarrow SF_5 + F \qquad (3.2.7c).$$

Obviously when dissociation occurs, there will be a drop in the neutral SF_6 concentration. From Section 1.3.3.(ii) it can be seen that at least six different gas reactions exist (excluding electron transfer reactions), which require the neutral SF_6 molecule for negative ion formation. It might be expected therefore that a loss of neutral SF_6 will reduce the net attachment rate. This could be expected if direct electron attachment to both SF_5 and F are inefficient processes in comparison to negative ion formation involving SF_6. No information appears to be available on direct electron attachment to SF_5. Presumably a vibrationally excited negative ion state ($(SF_5^-)^*$) is formed in this process. Whether stable SF_5^- ions will be formed from the excited ion, will depend on whether the life-time of $(SF_5^-)^*$ against autodetachment is large compared to the mean free time between molecular collisions at the pressures presently used. If the latter is not the case, then the $(SF_5^-)^*$ will suffer spontaneous detachment before it can be collisionally stabilized (see Section 1.3.3.(ii)). With regard to the fluorine atom, direct electron attachment could occur either by radiative or three-body attachment. It is likely however that the radiative capture cross-section of F^- is much smaller (as is that of SF_5^-) than the cross-sections for the attachment processes (reactions 1.3.3d and 1.3.3e) involving neutral SF_6. It can also be expected that at the low pressures presently used, the three-body attachment process will be insignificant.

The possibility of the current increase at time t_D being due to an increase in the rate of ionization cannot be excluded, but appears unlikely in view of the high ionization potential of F (18.6 eV). No information appears to be available regarding direct electron impact ionization of SF_5.

The onset of dissociation of SF_6 at time t_D, leading to a reduction in the attachment rate in the positive column, will provide an increase in discharge current. The increasing current will accelerate the rise in gas temperature and hence the rate of dissociation. This cumulative effect will lead to a rapid rise in discharge current and ultimately to the establishment of a new glow discharge phase, the dissociated glow. Compared to the preceding electronegative glow phase, the positive column of the higher current dissociated glow phase is maintained at a temperature high enough for substantial dissociation to occur. A further consequence of the higher temperature is a lower value of β, the ratio of the negative ion-to-electron concentration, in the column.

An increase in overvoltage increases the power input for the positive column during the transition process from time t_D to the final establishment of the dissociated glow. As observed, this decreases the duration of the transition, since the equilibrium temperature of the positive column is reached more rapidly. The dissociated glow current is also seen to increase with overvoltage. This suggests increased dissociation as a result of a higher equilibrium temperature in the column.

The high frequency noise and current instability which are observed to be initiated some time after the commencement of the current transition and which persist throughout the dissociated glow phase, are conspicuous on all the current and voltage oscillograms. Two possible causes are suggested for this instability. It may be that due to the increased concentration of fluorine atoms after dissociation, electrode-fluorine interactions in the form of anode and cathode spots, bring about the instability. This form of instability has been presently observed to occur in the constricted d.c. SF_6 discharge at high currents. An alternative possibility is that the instability is associated with variations in the direction of radial diffusion of the negative ions in the positive column. It is known (Arutunian and Galechian, 1979) that when the β-ratio falls below a critical value (which is

dependent on the positive (or negative) ion-to-electron mobility and temperature ratios) the direction of negative ion diffusion in the ambipolar field reverses from one of outward-going motion, to one directed inward towards the discharge axis. Calculations using the negative ion ambipolar diffusion equation of Arutunian and Galechian, show that for the present discharges at the time of the current transition, the critical β-value is of the order of 10^3 (taking $\frac{\mu_\pm}{\mu e} = 10^{-3}$, $T_e = 10^4$K and $T_\pm = T_{gas} = 10^3$K). The value of β in the dissociated glow phase is likely to be in the region of this critical value and radial oscillations of negative-ions could be a possible result.

When arcing does not take place, the current in the dissociated glow gradually decreases as the charge on the circuit capacitor is dissipated: this is seen in the current trace of Fig. 3.2.4.(iii). From Fig. 3.2.4.(v), it can be seen that from 2 to 12 ms after breakdown in the 0.8 Torr, 12 kV spark, a gradual decrease followed by another increase in the axial plasma refractivity occurs. The trough is presumably caused by rapid outward diffusion of the molecules (and atoms) under the large radial concentration gradient produced by dissociation. At this stage, a competition exists between the outward diffusion leading to a decrease in axial plasma refractivity, and dissociation leading to an increase.

After about 16 ms, the current in the 0.8 Torr, 12 kV spark has decreased appreciably, with a simultaneous cooling of the gas and reassociation. A decrease is thus observed in the gas refractivity. At about 24 ms after breakdown, the thyratron anode voltage collapses below the conduction maintenance value and the thyratron becomes open-circuited. As a result of this, a polarity reversal occurs across the discharge tube which induces current flow in the reverse direction. The current amplitude in this reversed phase is small ($\lesssim$ 1 mA) and cannot be resolved on the current trace of Fig. 3.2.4.(iii). During this phase, the axial plasma density continues to collapse and does so to a value below the original gas density, presumably due to continued outward diffusion. Restoration of the original insulating state then follows.

3.2.8 Some Further Supportive Evidence for the Occurrence of Attachment and Molecular Dissociation in the Glow Phases of the SF_6 Spark: The Study of SF_6/Argon Sparks

Further support for some of the effects of electron attachment and molecular dissociation in the SF_6 glow phases described in Sections 3.2.6.I, and 3.2.7, has been obtained by examining the effect of adding argon to the SF_6 discharges. Argon has been chosen in this study, on account of its inertness and because neither attachment nor dissociation occurs in it. Argon/SF_6 mixtures of total pressure 1 Torr have been pulsed in a 9 cm gap, using an applied voltage of 2.35 kV. The results obtained are shown in Fig. 3.2.8.(i) where the time-scale is logarithmic to highlight the variations in current. The oscillograms gradually vary in form between those for pure SF_6 and pure argon. They show how both processes are attenuated as the argon/SF_6 ratio increases. In the electronegative glow phase, as the argon content is increased, and attachment rates decrease, the currents in this phase become higher. With diminishing molecular content, the effect of dissociation, although it obviously still occurs, becomes less significant and the current rise into the dissociated glow phase, less distinct. The current trace for pure argon shows no sign of collapse and regrowth, but maintains a steady amplitude. In this quasistable phase, ionization is balanced by ambipolar diffusion losses (there is no attachment, and because the pressure is low, volume recombination losses are negligible).

Further evidence suggesting that the current collapse is due to electron attachment, was obtained when observing the shape of the argon current trace, after the electrodes were initially cleaned using a commercial degreasing agent. Under these conditions, a significant degree of collapse in the argon current trace was observed. It was subsequently found that the degreasing agent contained large quantities of "Freon" (C $C\ell_2F_2$/C $C\ell_2F_4$), which is highly electronegative (Meek and Craggs, 1978).

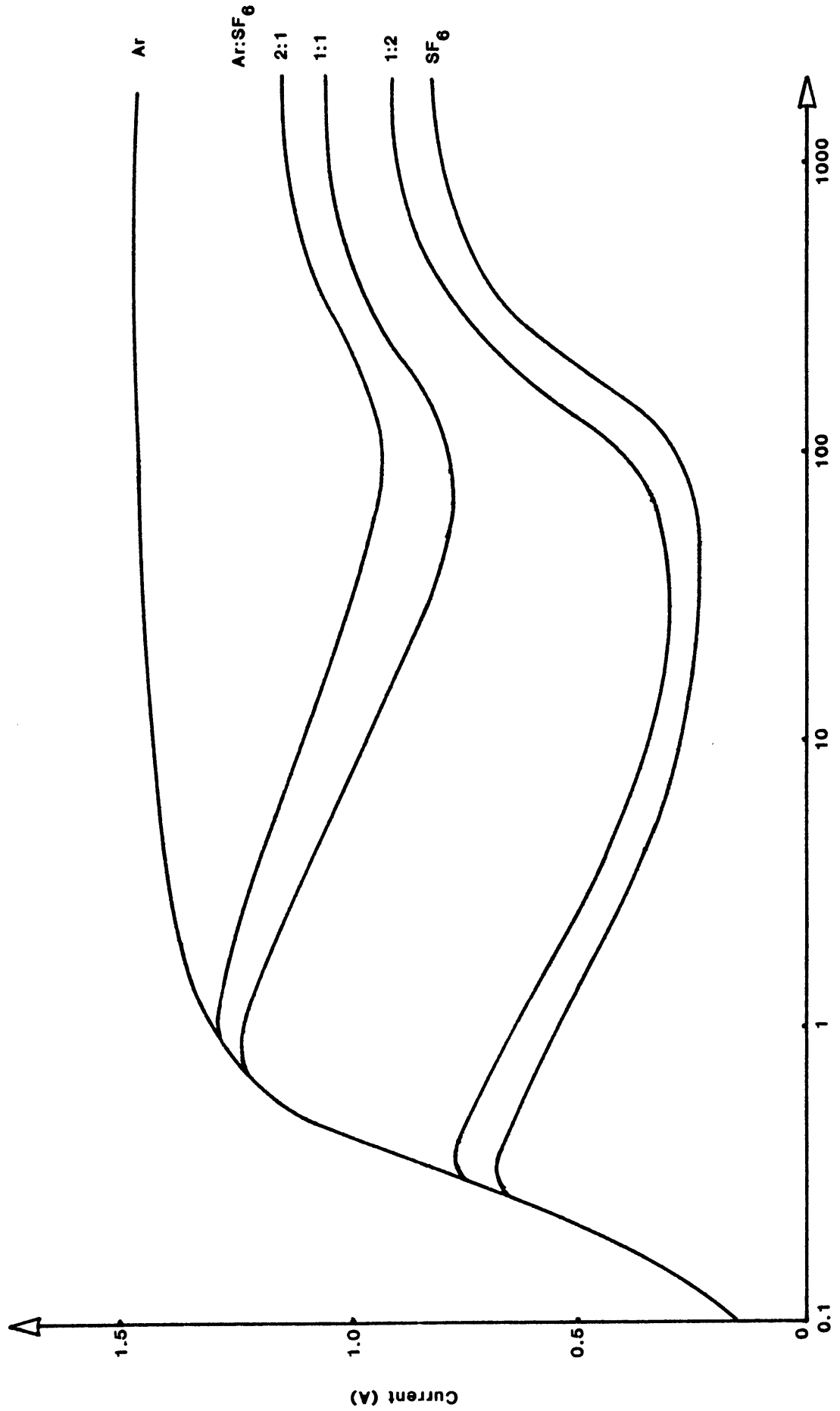

Fig. 3.2.8.(i) Growth of current curves in argon/SF_6 mixtures of total pressure 1 Torr, for an applied voltage of 2.35 kV and a gap length of 9 cm.

3.2.9 The Glow-Arc Transition, t_E-t_F

3.2.9.(i) Observations

By increasing the applied overvoltage above about 140% and keeping the external series resistance relatively small ($\sim$ 1 kΩ), it has been possible to generate the arc phase in the movable electrode chamber. To readily produce the glow-arc transition, however, it has been necessary also to use a special cathode rather than the stainless-steel disc electrode used for all the experiments described to this stage. As described in Section 2.1, this special cathode consists of a stainless-steel disc embedded in a machinable ceramic casing such that the front surface of the steel disc and casing are flush with one another.

Analysis of the glow-arc transition and the subsequent discharge has been made using current and voltage oscillograms, and electron micrographs of the cathode surface taken before and after the occurrence of a single spark which includes the glow-arc transition.

The glow-arc transition is represented in Figures 3.2.2.(i) and (ii) as the sudden discontinuity in current and voltage which is triggered during the dissociated glow phase at time t_E. As indicated in Section 3.2.2, the oscillogram of Fig. 3.2.2.(i) represents the current and voltage development in a 3.0 Torr, SF_6 spark pulsed at 3.0 kV in a 4.0 cm gap using the metal-ceramic cathode unit. The oscillogram shows that at the transition, the current increases from 600 mA to 1.5 A and the voltage collapses from -2100 volts to -1200 volts. This transition occurs in a time less than 20 ns, and is followed by a more gradual transition to a quasistable high current (2A) and relatively low voltage (600 volts) phase which becomes established at time t_F. A visual inspection of the cathode surface reveals that when the spark includes this high current, low voltage phase, a bright luminous spot always forms at the boundary between the metal cathode and the adjacent ceramic insulator. This observation is consistent with those made in an iodine spark when a metal-insulator cathode configuration is used (Lewis and Woolsey, 1981) - (see Section 1.2.2 of this thesis).

The time of occurrence of the glow-arc transition is found to be variable from shot-to-shot, and on some occasions it is observed to be triggered during the electronegative glow phase.

As indicated earlier, an electron-microscope photographic study has been made of the cathode surface. Before doing this, the discharge conditions were first set so that the transition could be readily obtained using the metal-ceramic cathode. Following this, a new metal-ceramic cathode of identical macroscopic dimensions, was made. This unit was polished with fine emery paper and then with "Brasso", and was subsequently dismantled into its metal and ceramic components and thoroughly washed in petroleum spirits and distilled ethanol. By doing this, most of the metal and ceramic shavings, and any grease lodged in the micro-crevices and on the exposed surfaces during manufacture, were eliminated. The unit was then re-assembled, washed again in distilled ethanol and thoroughly dried before inserting into the discharge chamber.

The SF_6 pressure, gap-length, applied voltage and series resistance were then set to 2.0 Torr, 4 cm, 3.0 kV and 1.0 kΩ, respectively, and a single discharge shot was fired. A luminous cathode spot was observed at a point on the metal-ceramic boundary. The current and voltage oscillograms showed an arc current of 2.5 A and an arc voltage of 500 volts. The transition occurred from the dissociated glow phase at a current of approximately 700 mA. It was observed however, that the arc was maintained for only about 1 ms before a collapse into the dissociated glow phase occurred. Then another glow-arc transition occurred and the arc phase was maintained again for another 500 ns, before gap recovery commenced. A voltage oscillogram is available, which shows the latter phenomenon in a 1.8 Torr SF_6 spark pulsed in a 6.5 cm gap at 3 kV. This is shown in Fig. 3.2.9.(i).

Following the single-shot experiment, the cathode unit was carefully removed from the discharge system and viewed under a Jeol scanning electron microscope (Model JSM-35). It was found that the central zones of the metal cathode were free of any markings due to the discharge. However, a number of micro-craters were observed in the peripheral zones. Most of the cathode

Fig. 3.2.9.(i) Oscillogram showing the voltage trace of a 1.8 Torr SF_6 spark pulsed in a 6.5 cm gap at an applied gap voltage of 3.0 kV and at an overvoltage of 150%.

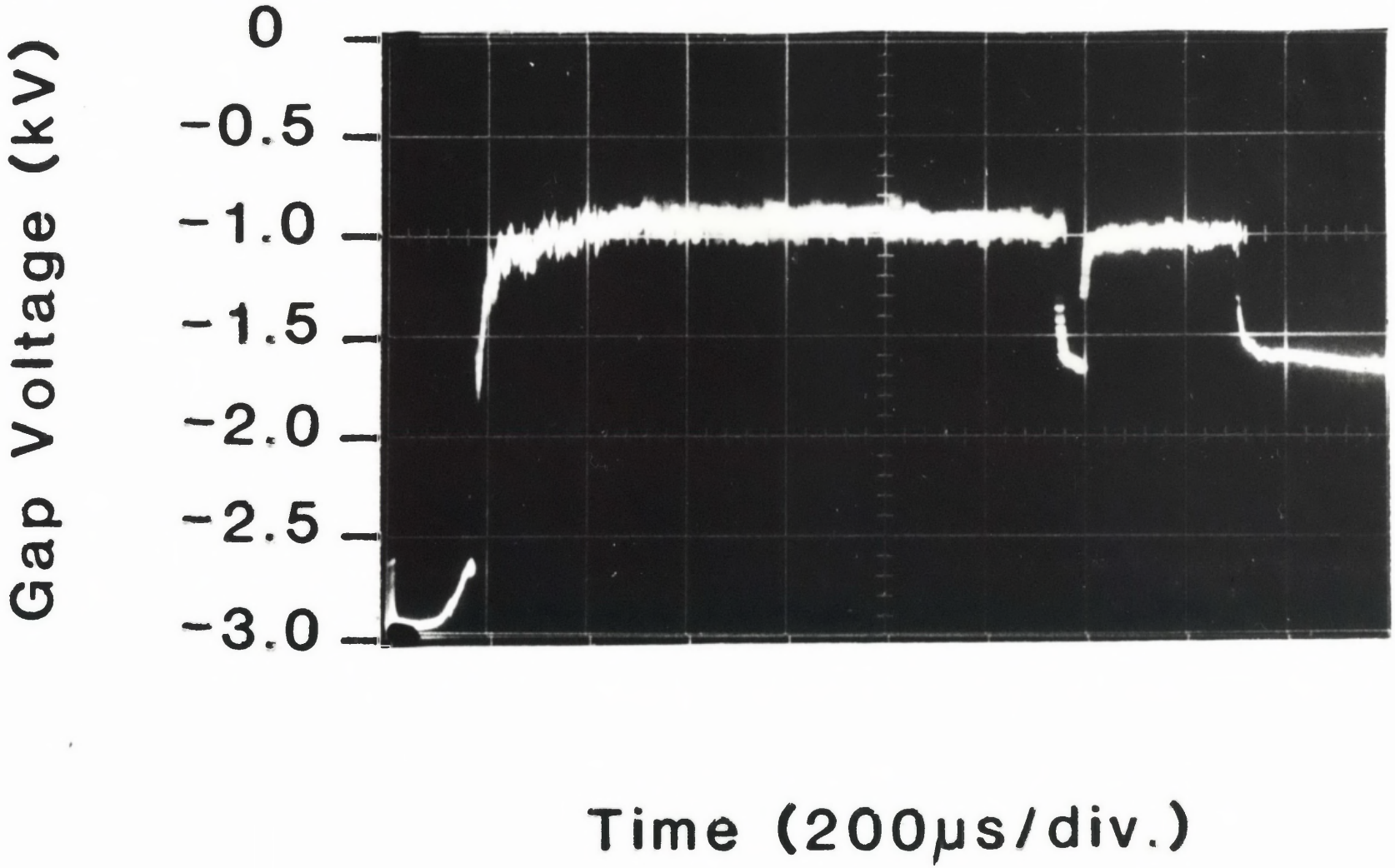
Gap Voltage (kV)
0
-0.5
-1.0
-1.5
-2.0
-2.5
-3.0
Time (200μs/div.)

Fig. 3.2.9.(ii) Electron micrograph showing a typical section of the cathode metal-insulator boundary, prior to sparking. The horizontal white line at the bottom of the micrograph represents a scale of 10 μm.

0 0 1 0 1 0 0

Fig. 3.2.9.(iii) Electron micrograph showing a region of the cathode metal-insulator boundary after one SF_6 spark. The scale shown represents a length of 100 μm.

Fig. 3.2.9.(iv) Electron micrograph showing another region of the metal-insulator boundary which has been affected by the same spark responsible for the melting shown in Fig. 3.2.9.(iii). The scale shown represents a length of 100 μm.

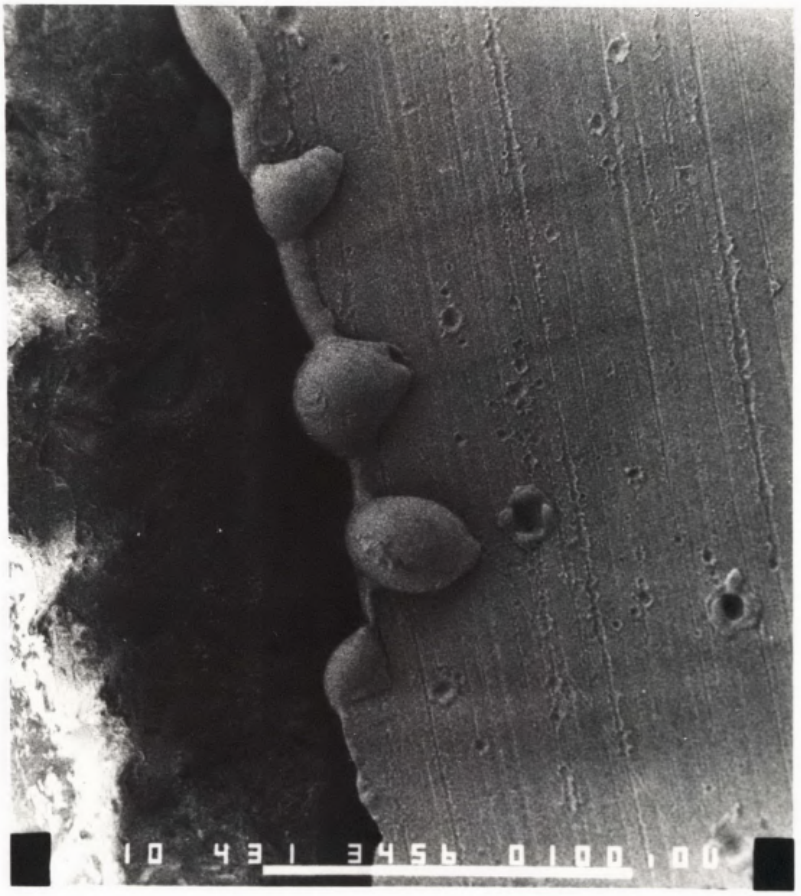
10 43 1 3456 0100,00

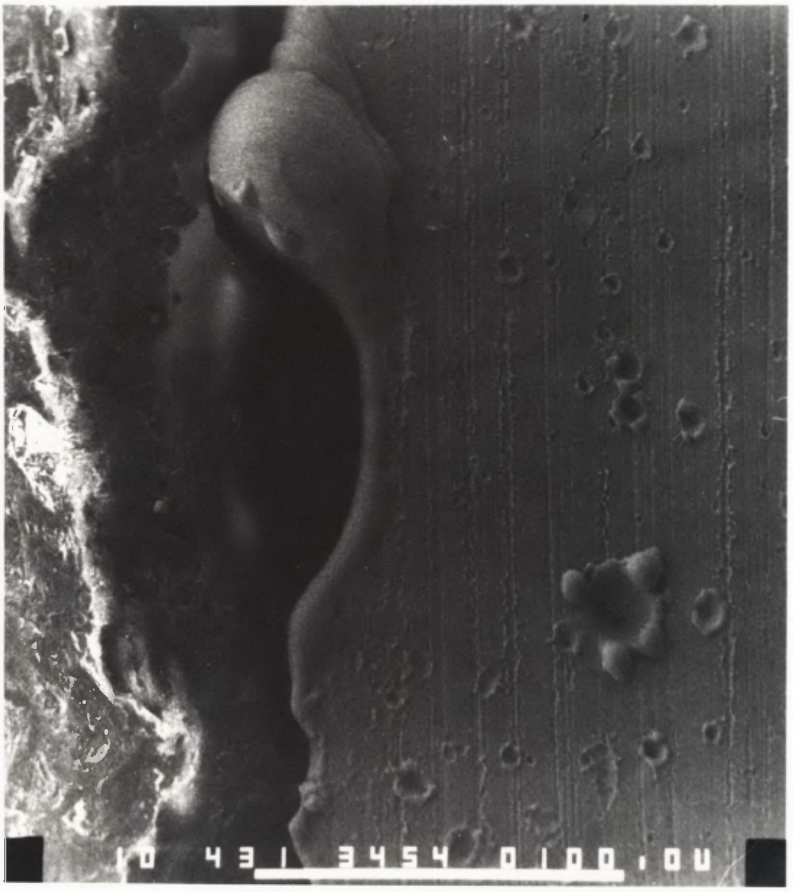
10 43 1 3454 0100,00

Fig. 3.2.9.(v) Electron micrograph showing the molten mound portrayed in Fig. 3.2.9.(iv) under larger magnification. The scale shown represents a length of 10 μm.

damage occurred at the metal-ceramic boundary in the vicinity of the observed cathode spot. The damaged boundary regions are shown in Figures 3.2.9.(iii), (iv) and (v). Figure (ii) shows a typical section of the boundary zone before the discharge was fired: the ceramic can be seen to be very uneven and jagged and a micro-crevice of about 25 μm in width is seen to separate the metal electrode from the adjacent ceramic. The metal is underexposed in this photograph because the cathode unit was not gold-filmed in the conventional manner (as was done, for example, in the case of Figures (iii), (iv) and (v), after the discharge shot was fired.). Nevertheless, the machine-cutting grooves and the sharp metal boundary are apparent in Fig. (ii). Figures (iii) and (iv) show the zone of cathode spot activity. Six distinct mounds, due to localized heating and melting are apparent. Five of these (Fig. (iii)) are interconnected by thin strips of boundary which have also suffered melting, while the sixth and largest mound (Fig. (iv)) exists on its own, some 500 μm along the boundary, away from the other five. No other mounds or signs of melting could be observed at any other location on the boundary. Figures (iii) and (iv) also show the micro-craters, and molten tracks coinciding with the original machining marks. The micro-craters vary in diameter from about 1 μm to 25 μm. Figure (v) shows the isolated mound of Fig. (iv) under greater magnification. It can be seen that the intense heating which has occurred, has also caused melting of the ceramic adjacent to this mound. From Fig. (iv) it can be seen how the cathode spot activity has carved away a section of the boundary and caused the molten metal to accumulate to one side, forming the mound.

3.2.9.(ii) Discussion

The sudden collapse in the gap voltage at time t_E, by the order of the cathode fall potential ($\sim$ 1000 volts) - (consider Fig. 3.2.2.(i)), together with the appearance of a cathode spot, suggests that a cathodic glow-arc transition occurs, which is characterised by a sudden change in the mechanism of cathode electron emission. An arc-cathode is likely to exist at this stage with the cathode fall collapsing to the order of the ionization potential of SF_6. The relatively large voltage ($\sim$ 600 volts) which remains across the gap

during the quasistable arc phase, however, suggests that thermal ionization in the positive column does not occur. If this process were to occur, the column field would collapse to the order of a few volts per cm. In the iodine spark, as studied by Lewis and Woolsey (1981), the gap voltage first collapses from -3 kV to -600 volts at the glow-arc transition, and then proceeds to collapse in a step-like manner to less than 50 volts when thermal ionization processes in the column have become established. At this stage the arc current is 5A and arc temperature, 5000 K. In the present work, as mentioned in (i), the gap voltage collapses from -2100 volts to -1200 volts at the sharp transition at time t_E, and then from -1200 volts to -600 volts by time t_F. A visual inspection of this spark indicates that the discharge is well constricted when the arc phase occurs, but is not filamentary as observed in iodine by Lewis and Woolsey. It appears therefore that in the present SF_6 spark, although the cathode processes change from glow to arc, the positive column remains glow-like, being controlled by electron-impact ionization rather than by thermal ionization. The combination of applied overvoltage ($\sim$ 150%) and series resistance (1 kΩ) act to limit the amount of energy delivered to the SF_6 arc phase. In the iodine spark of Lewis and Woolsey however, a larger applied overvoltage ($\sim$ 265%) and smaller series resistance (500 Ω) allow more energy to be supplied to the arc phase. This fact coupled with the fact that iodine has a thermal conductivity an order of magnitude smaller than that of SF_6 in the temperature range from 1000 K to 5000 K (Lewis, 1975), implies that the iodine spark heats up more efficiently, thus allowing the temperature to rise to the level at which thermal ionization processes become important ($\sim$ 5000 K - see Lewis and Woolsey, 1977). Heat losses in the SF_6 spark however, due to the relatively high thermal conductivity of SF_6 at about 1250 K for pressures of the order of 1 Torr (see Section 1.3.2), may serve to prevent the column temperature from rising to the thermal-ionization level. As a consequence, even though the column temperature is certainly high enough for thermal dissociation to occur, it remains controlled by electron-impact ionization processes.

The two possible mechanisms by which a cathodic glow-arc transition can occur are (i) thermionic emission or (ii) field emission. It seems unlikely

that thermionic emission triggers the glow-arc transition. This is because the currents flowing during the electronegative and dissociated glow phases are too small ($\sim$ mA) to provide sufficient energy to the cathode to raise its temperature high enough for thermionic emission to occur.

The regular appearance of cathode spots on the boundary between the metal and ceramic, suggests that the more likely mechanism by which the glow-arc transition is triggered, is by field emission. During the glow phase, the insulating ceramic surface adjacent to the metal cathode can become charged by positive-ion bombardment, so that the electric field at some point close to the cathode-insulator boundary eventually becomes large enough for field emission of electrons from the cathode to occur (Lewis and Woolsey, 1981). This is likely to happen at a point on the boundary where an irregularity in the cathode surface has already provided some electric field enhancement. Boyle and Haworth (1956) suggest that electrons emitted by field emission can lead to arc spot formation in the following way. Each field emission electron produces a small Townsend avalanche and the space-charge field thus created, enhances the existing cathode field. This induces further field emission, and the resulting cumulative process brings about the formation of a cathode spot and hence a glow-arc transition.

The high current density and resultant high temperature cathode spot result in the vaporization of metal and insulator at the boundary. A lower limit to the cathode emission current density after the transition, can be estimated from the current and the total melted area of the cathode surface. This measurement yields a lower limit since it is not known whether all the melted zones contribute simultaneously to the emission current during the arc phase. Further, Figures (iii) and (iv) suggest that the arc spot travels along the boundary (as is discussed below), so that the total melted area must yield a lower limit to the current density estimate. Neglecting the micro-craters on the cathode surface, the cathode current density is estimated using the approximate area of the melted boundary zones in Figures (iii) and (iv), to be of the order of $5 \times 10^8 \, A\,m^{-2}$. During the arc phase, it is expected

that there will be some contribution from thermionic emission due to the high temperatures produced at the cathode spot.

The time spent in the arc phase appears to depend on the availability of a high-field region at the cathode. It appears that the cathode spot travels around the metal-ceramic boundary, until it reaches a location where the field is too low to maintain the arc phase (for example, where the micro-crevice between the metal and ceramic is too wide, or the positive ion build-up on the ceramic is inadequate). When this occurs, the discharge returns to the dissociated glow phase until such time as the field at some point on the boundary is large enough to regenerate field emission and the glow-arc transition. Under the discharge conditions for which the electron micrographs were taken, two quasistable arc phases were observed before gap recovery occurred. It is suggested that the zone of boundary melting shown in Fig. (iii) is associated with one of these arc phases, while the independent zone of boundary melting shown in Fig. (iv) is connected with the other.

The micro-craters observed on the metal surface are probably due to localized field emission from thin layers of insulating impurity which have become externally charged up by positive ion bombardment. It has been observed in the present investigations that when a cathode with no metal-insulator boundary is used, numerous glow-arc transitions can sometimes be obtained, for which the arc duration is very short (of the order of only a few μs). This could be accounted for by the rapid vaporization of localized insulating films on the cathode surface due to field emission, and hence the rapid depletion of a high-field region required to maintain the arc phase. Under these conditions the discharge quickly returns to the dissociated glow phase where it remains until another suitably charged insulating film is available to produce field emission and the glow-arc transition.

The observation that the glow-arc transition in the low pressure SF_6 spark takes place at currents of the order of mA (as opposed to amperes in non-attaching gases - see for example, Figures 1.1.(ii),(iii)) can be accounted for in the same way as was done by Lewis and Woolsey (1981) for the iodine spark. As was

shown in Section 3.2.6.II, from Langmuir probe measurements in the low pressure and low current d.c. SF_6 discharge, the negative ion-to-electron number density ratio (β) in the electronegative glow phase of the spark is likely to be of the order of between 10^3 and 10^4. In Section 3.2.7, it was estimated that β would not collapse from this value by a significant factor, during the dissociated glow phase. Thus even though the spark current during the glow phases is only of the order of mA, a high positive ion flux may exist at the cathode, equivalent to that obtained at much higher currents in glow discharges through non-attaching gases. The glow-arc transition at such low currents can thus be understood, since the field emission mechanism depends not on the total discharge current, but on the degree of positive ion bombardment.

3.2.10 Summary and General Conclusions

The use of time-resolved oscillographic and interferometric techniques has allowed the various phases of the low pressure SF_6 spark to be studied. In addition, an investigation of the low pressure d.c. SF_6 glow discharge has made it possible to interpret some phenomena common to both the spark and d.c. forms of glow discharge.

The findings made in the present work with regard to the low pressure SF_6 spark can be summarized as follows.

The statistical time-lags to breakdown in SF_6 are significantly reduced by continuous u.v. irradiation of the discharge gap. This can be accounted for by the availability of suitably located initiatory electrons at the instant of gap voltage application, due to photodetachment of negative ions.

Upon breakdown, the discharge current sharply increases and then suddenly decreases to a low amplitude, quasistable glow phase (the electronegative glow phase) for a time which is inversely proportional to the rate at which energy is delivered to the gap from the external circuit. The transition into this low current phase is accounted for in terms of a reduction in the column field during the space-charge phase and hence by the rapid increase in the rate of electron attachment due to a decrease in the mean electron energy. The negative ion-to-electron number density ratio (β) in this phase is in excess of 10^3 as shown from Langmuir probe measurements made in the equivalent low pressure and low current d.c. SF_6 glow discharge. The 'electronegativity' of this phase has also been demonstrated by the effect of adding argon, a non-attaching gas, to the SF_6 discharge.

A current pulse phenomenon observed in the electronegative glow phase under specific conditions of applied overvoltage and discharge current, occurs also at similar currents in the d.c. SF_6 discharge. The experimental evidence obtained from measurements of the positive column E/N-values, shows that the current pulses occur at a critical mean electron energy of approximately 11eV. Further, a spectroscopic investigation reveals that the discharge light

is dominated by the nitrogen second positive band system during the current pulses. It is concluded on the basis of this and other evidence that the current pulses are the result of electron production through photodetachment of negative ions by the u.v. radiation from nitrogen impurity molecules. It is estimated that the air (nitrogen) impurity has to be in excess of about 1 part in 10^4 of SF_6 in order for the current pulses to occur.

Interferometric measurements of absolute particle densities in the SF_6 spark indicate that the current increase at the end of the low current phase is accompanied by a considerable degree of molecular dissociation. This is supported by interferometric measurements of absolute number density variations in hydrogen sparks pulsed at both high and low overvoltages. The measurements at high overvoltage show a sharp increase in the particle number density following an initial decrease, as in SF_6, while measurements in hydrogen at low overvoltages show that the temporal variation of the plasma refractivity is more like that of argon, in which dissociation cannot occur. It has also been shown from an energy calculation that the gas temperature at the time of the current increase in the central core of the SF_6 spark, is sufficient for thermal dissociation of the SF_6 molecules to occur. The current increase into the dissociated glow phase of the SF_6 spark can be accounted for by a reduction in the overall attachment rate, through the loss of SF_6 molecules by dissociation. This is possible if direct electron attachment to SF_5 and F are inefficient processes compared to negative ion formation involving neutral SF_6.

The electronegative and dissociated glow phases appear to be abnormal glows. Both have high cathode fall potentials and relatively low discharge currents.

At percentage overvoltages in excess of 150%, the arc phase can be obtained provided a small enough series resistance is used. The presence of an insulating casing around the metal cathode encourages the glow-arc transition. A field emission mechanism assisted by the charging up of the

insulating surfaces in the vicinity of the cathode metal boundary, appears to bring about the transition.

The comparatively large gap voltage which remains during the arc phase ($\sim$ 600 volts) suggests that the positive column remains controlled by electron-impact ionization as opposed to thermal ionization. In other words, the positive column during the arc phase remains glow-like, although an arc cathode exists.

The work of this thesis by no means provides a complete description of the low pressure SF_6 spark, and considerable potential exists with regard to future work.

In particular, future studies will benefit enormously from the use of time-resolved photography and spectroscopy. Photography will provide details of changes in discharge structure, which can often be useful in the determination of the processes controlling the behaviour of quasistable phases and the transitions between them. Spectroscopy will help in determining the dominant atomic and molecular species at various stages of the spark, as well as providing information on impurity levels.

The use of an ultra-high vacuum system together with a fine control gas inlet arrangement would allow a more critical study to be made of the role of small additions of nitrogen and other gases.

Particular phases and transitions of the SF_6 spark which require further experimental study include the transition from the space-charge phase to the electronegative glow phase; the dissociated glow phase and in particular the current instability phenomenon; and the glow-arc transition.

As already indicated in the introduction of this thesis, very little work has been done on the d.c. glow discharge in SF_6. The d.c. glow has been used in the present work only as an aid to the investigation of certain aspects of the glow phases of the SF_6 spark. It has been shown however that negative ions do play a crucial role in d.c. SF_6 glow discharges. The present work

demonstrates also that several diagnostic techniques including Langmuir probes and interferometry, can be used to provide quantitative data on attachment processes in SF_6 glow discharges. Further exploitation of these techniques should lead to detailed information becoming available on d.c. SF_6 glows, both on the lower current molecular glow, and on the higher current glow in which appreciable dissociation takes place.

BIBLIOGRAPHY

Ahearn, A.J. and Hannay, N.B.

1953 J. Chem. Phys. 21, 119.

Allen, K.R. and Phillips, K.

1964 Proc. Roy. Soc. 278A, 188.

Alpher, R.A. and White, D.R.

1959 Phys. Fluids. 2, 162.

1965 Plasma Diagnostic Techniques, ed. Huddlestone, R.H. and Leonard, S.L. (Academic Press), 431.

Arutunian, G.G. and Galechian, G.A.

1979 Proc. 14th Int. Conf. Phenomena Ionized Gases, C7-205.

Bayle, M., Bayle, P. and Gayraud, F.

1977 J. Phys. D.: Appl. Phys. 10, 2181.

Bayle, P. and Bayle, M.

1964 Z. Phys. 266, 275.

Berry, R.S. and Reimann, C.W.

1963 J. Chem. Phys. 38, 1540.

Bhalla, M.S. and Craggs, J.D.

1962 Proc. Phys. Soc. 80, 151.

Biondi, M.A. and Fox, R.E.

1958 Phys. Rev. 109, 2012.

Blackwell, B.D., Cross, R.C. and Falconer, I.S.

1979 J. Phys. E.: Sci. Instrum. 12, 39.

Born, M. and Wolf, E.

1975 Principles of Optics (Pergamon).

Boyle, W.S. and Haworth, F.E.

1956 Phys. Rev. 101, 935.

Brabenec, M.K. and Williams, A.W.

1972 Proc. 2nd Int. Conf. Gas Discharges (IEE), 332.

Brokaw, R.S.

1960 J. Chem. Phys. 32, 1005.

Browne, T.E.

1948 Trans. Amer. Inst. Elect. Engrs. 67, 141.

Buss, K.

1930 Arch. Elektrotech. 26, 266.

Capitelli, M. and Devoto, R.S.

1973 Phys. Fluids 16, 1835.

Cavenor, M.C. and Meyer, J.

1969 Aust. J. Phys. 22, 155.

Chalmers, I.D., Duffy, H. and Tedford, D.J.

1972 Proc. R. Soc. Lond. 329A, 171.

Chalmers, I.D. and Tedford, D.J.

1975 J. Phys. D.: Appl. Phys. 8, 943.

Chantry, P.J. and Chen, C.L.

1976 Bull. Am. Phys. Soc. 21, 170.

Chen, C.L. and Chantry, P.J.

1970 Bull. Am. Phys. Soc. 15, 418.

Cobine, J.D.

1941 Gaseous Conductors (McGraw-Hill)

Compton, R.N., Christophorou, L.G., Hurst, G.S. and Reinhardt, P.W.

1966 J. Chem. Phys. 45, 4634.

Compton, R.N., Nelson, D.R. and Reinhardt, P.W.

1971 Int. J. Mass Spectrom. Ion. Phys. 6, 117.

Cookson,A.H. and Farish, O.

1973 I.E.E.E. Trans., PAS-92, 871.

Cooper, J.W. and Martin, J.B.

1962 Phys. Rev. 126, 1482.

Craggs, J.D. and Meek, J.M.

1962 Proc. Int. Conf. on Gas Discharges and Electrical Supply Industry, 338.

Crichton, B.H., Ibrahim, O.E. and Farish, O.

1976 Proc. 4th Int. Conf. Gas Discharges (IEE), 117.

Davies, A.J., Davies, C.S. and Evans, C.J.

1971 Proc. Inst. Electr. Eng. 118, 816.

Davies, A.J., Donne, K.E. and Hill, C.J.

1976 Proc. 4th Int. Conf. Gas Discharges (IEE), 176

Davies, A.J., Evans, C.J. and Woodison, P.M.

1975 Proc. Inst. Electr. Eng. 122, 765.

Dehne, K., Kohrmann, W. and Lenne, H.

1963 Dielectrics 1, 129.

Dibeler, V.H. and Mohler, F.L.

1948 J. Res. Nat. Bur. Stand. 40, 25.

Dibeler, V.H. and Walker, J.A.

1966 J. Chem. Phys. 44, 4405.

Doran, A.A.

1968 Z. Phys. 208, 427.

1969 Aust. J. Phys. 22, 447.

Doran, A.A. and Meyer, J.

1967 Brit. J. Appl. Phys. 18, 793.

Eccles, M.J.

1968 Ph.D. Thesis, University of Liverpool

Eccles, M.J., O'Neill, B.C. and Craggs, J.D.

1970 J. Phys. B.: Atom. Molec. Phys. 3, 1724

Eccles, M.J., Prasad, A.N. and Craggs, J.D.

1967 Electron. Lett. 3, 410.

Edelson, D., Griffiths, J.E. and McAfee, K.B., Jr.

1962 J. Chem. Phys. 37, 917.

Emeleus, K.G. and Sayers, J.

1938 Proc. Roy. Irish Acad. 44A, 87.

Emeleus, K.G. and Woolsey, G.A.

1970 Discharges in Electronegative Gases (Taylor and Francis)

Farish, O.

1982 Proc. 2nd Gaseous Electronics Meeting (University of New England) - (unpublished paper).

Farish, O. and Tedford, D.J.

1967 Proc. Inst. Electr. Eng. 114, 277.

Fehsenfeld, F.C.

1970 J. Chem. Phys. 53, 2000.

1971 J. Chem. Phys. 54, 438.

Francis, G.

1956 Handbuch der Physik, ed. Flugge, S. (Springer-Verlag), 53.

Francon, M.

1966 Optical Interferometry (Academic Press).

Frie, W.

1967 Z. Phys. 201, 269.

Frind, G.

1960 Z. Angew Phys. 12, 231.

Frost, L.S. and Liebermann, R.W.

1971 Proc. I.E.E.E. 59, 474.

Gambling, W.A. and Edels, H.

1954 Brit. J. Appl. Phys. 5, 36.

Garscadden, A.

1978 Gaseous Electronics, Vol. 1: Electrical Discharges, eds. Hirsh, M.N. and Oskam, H.J. (Academic Press), 65.

Gaydon, A.G. and Hurle, I.R.

1963 The Shock Tube in High-Temperature Chemical Physics (Chapman and Hall).

Geballe, R. and Reeves, M.L.

1953 Phys. Rev. 92, 867.

Ghosh, A.K., Carswell, A.I. and Richard, C.

1967 Phys. Fluids 10, 1100.

Gockenbach, E.

1976 Proc. 4th Int. Conf. Gas Discharges (IEE), 113.

Gray, E.W., Coulter, J.R.M. and Emeleus, K.G.

1966 Electronics Lett. 2, 30.

Henis, J.M.S. and Mabie, C.A.

1970 J. Chem. Phys. 53, 2999.

Hertz, W., Motschmann, H. and Wittel, H.

1971 Proc. I.E.E.E. 59, 485.

Hickam, W.M. and Fox, R.E.

1956 J. Chem. Phys. 25, 642.

Hirsh, M.N. and Oskam, H.J.

1978 Gaseous Electronics, Vol. 1: Electrical Discharges (Academic Press).

Hotop, H. and Lineberger, W.C.

1975 J. Phys. & Chem. Ref. Data. 4, 539.

Huxley, L.G.H. and Crompton, R.W.

1974 The Diffusion and Drift of Electrons in Gases (Wiley).

Imami, M. and Borst, W.L.

1974 J. Chem. Phys. 61, 1115.

Ishihara, T. and Foster, T.C.

1974 Phys. Rev. A9, 2350.

Ishikawa, I. and Suganomata, S.

1976 Japan J. Appl. Phys. 15, 1855.

Ishikawa, I., Suganomata, S. and Matsumoto, M.

1979 Phys. Lett. 73A, 319.

J.A.N.A.F. Thermochemical Data

1965 (Dow Chemical Company).

Kekez, M.M., Barrault, M.R. and Craggs, J.D.

1970 J. Phys. D.: Appl. Phys. 3, 1886.

1972 J. Phys. D.: Appl. Phys. 5, 253.

Kekez, M.M. and Savic, P.

1974 J. Phys. D.: Appl. Phys. 7, 620.

1975 Proc. 12th Int. Conf. Phenomena in Ionized Gases, 161.

1976 Proc. 4th Int. Conf. Gas Discharges, 129.

Kiang, T., Estler, R.C. and Zare, R.N.

1979 J. Chem. Phys. 70, 5343.

King, L.A.

1954 Nature, Lond. 174, 1008.

Kline, L.E.

1974 J. Appl. Phys. 45, 2046.

Kline, L.E., Davies, D.K., Chen, C.L. and Chantry, P.J.

1979 J. Appl. Phys. 50, 6789.

Köhrmann, W.

1964 Z. Naturf. 19a, 926.

Kuffel, E. and Radwan, R.O.

1966 Proc. Inst. Electr. Eng. 133, 1863.

Langmuir, I. and Mott-Smith, H.M.

1924 Gen. Elect. Rev. 27, 449.

Lee, P.H. and Woolsey, G.A.

1981 Appl. Optics, 20, 3514.

Lewis, D.B.

1975 Ph.D. Thesis, University of New England.

Lewis, D.B. and Woolsey, G.A.

1971 Proc. 10th Int. Conf. Phenomena in Ionized Gases, 159.

1977 J. Chem. Phys. 66, 1656.

1981 J. Phys. D.: Appl. Phys. 14, 1445.

Lifshitz, C., Tiernan, T.O. and Hughes, B.M.

1973 J. Chem. Phys. 59, 3182.

1980 J. Chem. Phys. 72(1), 789.

Lifshitz, C. and Weiss, M.

1972 Chem. Phys. Lett. 15, 266.

Loeb, L.B. and Meek, J.M.

1940 J. Appl. Phys. 11, 438.

Lowke, J.J. and Liebermann, R.W.

1971 J. Appl. Phys. 42, 3532.

McAfee, K.B. and Edelson, D.

1963 Proc. Phys. Soc. 81, 382.

McDaniel, E.W.

1964 Collision Phenomena in Ionized Gases (Wiley & Sons).

McGeehan, J.P., O'Neill, B.C., Prasad, A.N. and Craggs, J.D.

1975 J. Phys. D.: Appl. Phys. 8, 153.

Maecker, H.

1964a An Introduction to Discharge and Plasma Physics, ed. Haydon, S.C.
1964b (University of New England Press), 245, 259.

Mahan, B.H. and Young, C.E.

1966 J. Chem. Phys. 44, 2192.

Mandl, A.

1971 Phys. Rev.A 3, 251.

Marode, E. and Bastien, F.

1978 Proc. 5th Int. Conf. Gas Discharges (IEE), 343.

Marriott, J.

1954 Ph.D. Thesis, University of Liverpool.

Marriott, J. and Craggs, J.D.

1956 British J. Electronics, (IV) 1, 405.

Massey, H.

1976 Negative Ions (Cambridge University Press).

Meek, J.M.

1940 Phys. Rev. 57, 722.

Meek, J.M. and Craggs, J.D.

1978 Electrical Breakdown of Gases (Wiley & Sons).

Naidu, M.S. and Prasad, A.N.

1970 J. Phys. D.: Appl. Phys. 3, 951.

1972 J. Phys. D.: Appl. Phys. 5, 983.

Nielsen, T.M. and Pedersen, A.

1972 Proc. 2nd Int. Conf. Gas Discharges (IEE), 323.

O'Neill, B.C. and Craggs, J.D.

1973 J. Phys. B.: Atom. Molec. Phys. 6, 2634.

Odom, R.W., Smith, D.L. and Futrell, J.H.

1974 Chem. Phys. Lett. 24, 227.

Patterson, P.L.

1969 Proc. 22nd Gas Electron. Conf. 97

Pearse, R.W.B. and Gaydon, A.G.

1976 The Identification of Molecular Spectra (Chapman & Hall), 219.

Pedersen, A.

1970 I.E.E.E. Trans. Pwr. Appar. Syst. PAS-89, 2043.

Pfeiffer, W. and Schmitz, W.

1978 Proc. 5th Int. Conf. Gas Discharges (IEE), 328.

Plumb, I.C., Woolsey, G.A. and Lewis, D.B.

1973 Proc. 11th Int. Conf. Phenomena in Ionized Gases, 431.

Prasad, A.N. and Craggs, J.D.

1965 Electron. Lett. 1, 118.

Raether, H.

1939 Z. Phys. 112, 464.

1940 Arch. f. Elektrotek 34, 49.

1964 Electron Avalanches and Breakdown in Gases (Butterworths).

Rees, J.A.

1973 Electrical Breakdown in Gases (MacMillan).

Reich, H.J.

1939 Theory and Applications of Electron Tubes, 311 (McGraw-Hill).

Rescigno, T.N., Bender, C.F. and McKoy, B.V.

1978 Phys. Rev. A17, 645.

Robinson, E.J. and Geltman, S.

1967 Phys. Rev. 153, 4.

Rogoff, G.L.

1972 Phys. Fluids 15, 1931.

Rogowski, W., Flegler, E. and Tamm, R.

1927 Arch. Elektrotech 18, 479.

Sasanuma, M., Ishiguro, E., Hayaisha, T., Masuko, H., Morioka, Y., Nakajima, T. and Nakamura, M.

1979 J. Phys. B.: Atom. Molec. Phys. 12, 4057.

Schlumbohm, H.

1962 Z. Phys. 166, 192.

Schmidt, M. and Siebert, W.

1973 Comprehensive Inorganic Chemistry 2, 846 (Pergamon).

Schumb, W.C.

1947 Industrial and Engineering Chemistry 39, 421.

Seeliger, R.

1944 Einführung in die Physik der Gasentladungen, 133 (Edwards Brothers, Inc.).

Somerville, J.M.

1964 An Introduction to Discharge and Plasma Physics, ed. Haydon, S.C. (University of New England Press), 241.

Spencer-Smith, J.L.

1935a Phil. Mag. 19, 806.

1935b Phil. Mag. 19, 1016.

Suganomata, S. and Ishikawa, I.

1978 Japan J. Appl. Phys. 17, 1441.

Suleebka, P., Barrault, M.R. and Craggs, J.D.

1975 J. Phys. D.: Appl. Phys. 8, 2190.

Swarbrick, P.

1967 Brit. J. Appl. Phys. 18, 419.

Tholl, H.

1967 Z. Naturf. 22a, 1068.

von Engel, A.

1965 Ionized Gases (Oxford University Press).

Wagner, K.H.

1966 Z. Phys. 189, 465.

1967 Z. Phys. 204, 177.

Ward, A.L.

1965 Phys. Rev. 138A, 1357.

Woolsey, G.A.

1963 Proc. 6th Int. Conf. Phenomena in Ionized Gases, 141.

Woolsey, G.A., Emeleus, K.G., Brown, J.M., McCloskey, J.J.G. and Coulter, J.R.M.

1965 Int. Journ. Electronics 19, 485.

Woolsey, G.A. and Illingworth, R.

1972 J. Phys. E.: Sci. Instrum. 5, 575.

Woolsey, G.A., Plumb, I.C. and Lewis, D.B.

1973 J. Phys. D.: Appl. Phys. 6, 1883.

Yos, J.M.

1963 AVCO Tech. Mem. RAD-TM-63-7, ASTIA Doc. AD-435-053.